The Pennsylvania State University

The Graduate School

John and Willie Leone Family Department of Energy and Mineral Engineering

INVESTIGATIONS OF GAS SORPTION-INDUCED STRAIN FOR SORPTIVE ROCKS USING A NEW OPTICAL METHOD

A Thesis in

Energy and Mineral Engineering

by

Xu Zhao

Submitted in Partial Fulfillment
of the Requirements
for the Degree of

Master of Science

December 2015

The thesis of Xu Zhao was reviewed and approved* by the following:

Shimin Liu

Assistant professor of Energy and Mineral Engineering

Thesis Adviser

Derek Elsworth

Professor of Energy and Geo-Environmental Engineering

Ming Xiao

Associate Professor of Civil Engineering

Luis F. Ayala H.

Professor of Petroleum and Natural Gas Engineering;

Associate Department Head for Graduate Education

*Sigatures are on file in the Graduate School

ABSTRACT

It was a well-known phenomenon that the adsorption of sorbing gas results in change of coal matrix volume due to the surface energy change. The changes of matrix volume would affect the permeability in coal during CBM production and have impact on CO_2 coalbed sequestration. Shale, as a sorptive rock, is expected to have similar sorption-induced change of matrix volume. Besides its influence on permeability, the change of matrix volume would also change stress status in formation, thus affecting well stability. Therefore, a thorough understanding of sorption-induced strain in coal and shale is critical for the energy bearing subsurface characterization.

In this study, an optical-based strain measurement apparatus was designed and established to measure the areal strain of specimens of San Juan coal, Hazelton coal and Marcellus shale with carbon dioxide and helium injections. For coals, compared with strain gauge, this optical method avoids the use of chemical glue and reduces the influence of the built-in cleats. At 5 MPa CO_2, the linear strain of San Juan coal is 0.7% in current work but the value measured by pervious researchers using strain gauges is 0.37%, which is expected.

The areal strain results for San Juan coal and Hazelton coal follows the Langmuir-type equation. Liu and Harpalani model was also used to model the

pressure-strain data and the modeled results well matched with the measured strain data by choosing proper rock properties. The swelling of Hazelton coal with CO_2 is greater than that of San Juan coal at low pressure (<2.48MPa), and lower than that of San Juan coal at high pressure (>2.48MPa), which means the swelling depends not only on rank but also on other petrophysical properties.

For Marcellus shale specimens, a negative strain was observed with CO_2 at low pressure (0.69MPa). This repeatable results might imply that the adsorption-induced swelling was fully offset by the mechanical compression at low pressure. With injection pressure increase, the adsorption-induced strain started to dominate the overall strain behavior and a maximum swelling strain of 0.18% was observed for the tested shale.

TABLE OF CONTENTS

List of Figures

List of Tables

ACKNOWLEDGEMENTS

I would like to express my deepest appreciation and thanks to my advisor, Dr. Shimin Liu. As my teacher, he has provided me with great support for my research. As my mentor, he gives me a lot of ideas about life and makes me think differently. This research wouldn't have been completed without his help.

I would like to thank my co-worker, Benjamin Adams, PhD student in the Department of Civil and Environmental Engineering. He gave me a lot of help as an expert in image processing. Some ideas were come up with from discussion with him.

I also would like to thank my colleagues, Rui Zhang, Yi Wang, and Yang Wang. Without their help, the thesis will not be complete as it is.

My appreciation also goes to Dr. Ming Xiao who provides the experimental facility in imaging analysis and advice.

Here, I use this opportunity to thank my parents and friends for their love and support throughout my master's work.

CHAPTER ONE

INTRODUCTION

1.1 Coalbed Methane and Shale Gas Production

Coalbed methane (CBM) is an important part of natural gas in America. The commercial production started in early 1980s. Figure 1.1 shows the historical CBM production from 1989 to 2013 based on the data from Energy Information Administration (EIA). Although slightly decrease in recent a few years, the overall trend of CBM production was increasing in the past 3 decades. The coalbed methane production in 2013 was 1.47 trillion cubic feet (TCF) and account for 6% of the U.S. dry natural gas production (EIA, 2015). The latest data from EIA suggests that proven CBM reserves of U.S. was 12.4 TCF in 2013. Besides U.S., other countries, such as China, Canada, Indonesia, and Australia, have increasing interest in CBM development.

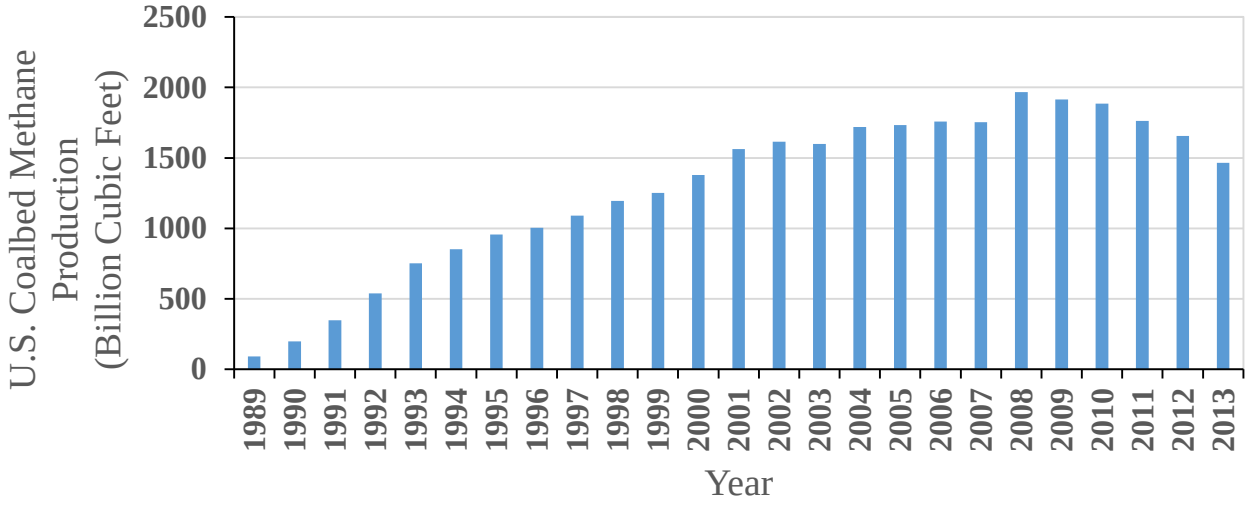

Figure 1.1: Historical coalbed methane production (EIA, 2014).

Shale gas is rapidly increasing as an available source of natural gas in America. Let by new applications of hydraulic fracturing and horizontal drilling, the reserves of shale gas was

increasing largely in past few years. EIA reports that the proved reserves in 2013 was 159.1 trillion cubic feet which was 6.83 times of reserves in 2007. Figure 1.2 shows the historical shale gas production from 2007 to 2013. The shale gas production in 2013 was 11.4 trillion cubic feet (TCF) which accounts for 46.5% of the U.S. dry natural gas production (EIA, 2015).

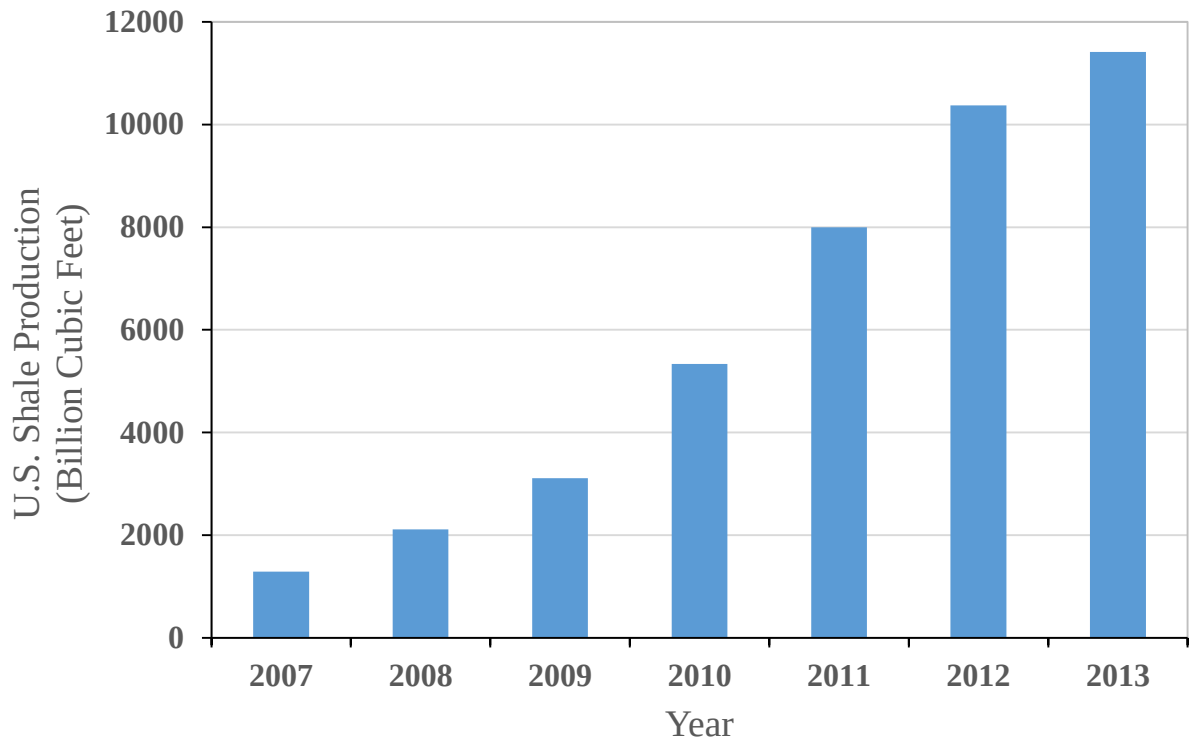

Figure 1.2: Historical shale gas production (EIA, 2014)

Both coalbeds and gas shale reservoirs are classified as unconventional gas reservoir because of their atypical geological conditions. Coalbeds are featured by dual porosity and gas shale reservoirs are very tight.

1.2 Problem Statement

Some experimental and theoretical work have suggested that the permeability of coal is affected by volumetric change of matrix. Several authors (Heller and Zoback, 2014; Cui et al., 2009; Ross and Bustin, 2007) have suggest the importance of adsorption-induced deformation of shale. However, the relationships between volumes of gas shale or coal and fluid pressure are not clearly understood.

Especially for gas shale, the volumetric response of matrix is rarely realized. Coal and gas shale are both sorptive geo-materials due to the inclusion of sorptive minerals such as organic matter and clays. The volumetric response of matrix, therefore, comes from mechanical compression and sorption-induced swelling/ shrinkage.

A lot of researchers have made effort to understand the adsorption-induced deformation in coal matrix (Moffat and Weale, 1955; Harpalani and Schraufnagel, 1990; Seidle and Huitt, 1995; Levine, 1996; Harpalani and Chen, 1997). Such information for gas shale, however, is very limited and literature is absence for the volumetric response of gas shale matrix.

In pervious laboratory work, large-sized blocks were used to be measured and strain gauges were the typical tools for measurement. There are mainly two problems within pervious work. The first one is that a lot of cleats were included in surface where strain gauges were stuck. The second one is that relatively thick layer of glue was used to stick strain gauges. Both problems would result in inaccuracy of measurement of matrix deformation. Hence, an optical measurement apparatus was developed to overcome those problems. It will give us more precise strain data and improve the understanding of volumetric response of coal/ shale matrix with sorbing environment.

1.3 Organization of Thesis

The thesis is organized into six chapters. In order to address the problem well, a wide background about coal and gas shale needs to be introduced. Also it is critical to have a sound knowledge of gas storage and transport mechanism. Therefore, Chapter 2 provides important background regarding coal and gas shale. Information, such as physical structure, origin, and composition is provided here. Besides, the storage and transport mechanisms of gas in coalbed and gas shale are described here.

Chapter 3 reviews the previous experimental and theoretical work about the adsorption-induced strain in CBM reservoirs. The swelling of minerals in gas shale was described briefly in chapter 3.

Chapter 4 presents an experimental plan with the setup of new designed optical-based strain measurement apparatus and the procedure of the experiment. Besides, the relationship between volumetric strain and areal strain is demonstrated here.

Chapter 5 presents the results in the experiment and the discussion about the results. Some calculations are based on the assumptions in previous work. Langmuir-type model and a theoretical model (Liu and Harpalani, 2013) were used to fit the experimental data.

Chapter 6 makes the conclusions drawn based on the experimental data, modeling results and discussion. Some recommendations are also provided for future work.

CHAPTER 2

BACKGROUND

2.1 Fundamentals of Coal

Coal is defined as a rock composed of more than 50% organic matter by weight and is thus by definition the rock type that is richest in organic matter (Pashin, 2008). Therefore, coal is thought to be an important petroleum source rock. The natural gas produced by coal is usually called coalbed methane which accounts for 6% of dry natural gas in US in 2013 and has been commercialized around the world for about three decades (Pashin, 2008). The uniqueness of storage and transport mechanisms makes coalbed methane different from other conventional natural gas reservoirs such as sandstone and carbonate reservoirs. Because of the richness in organic matters, the stress-strain relationship for coal is different from other rocks that coal matrix, defined as the solid skeleton of the coal, can shrink and/or swell with sorption gas(es). This shrinkage/swelling phenomenon is critical for gas transport modeling as it determines the pore-solid structure dynamics. In order to better realize the volumetric behavior of coal matrix in different gas environments, the characteristics of coal need to be understood clearly.

2.1.1 Coal Origin

Coal is universally thought to be vegetal in origin (Haenel, 1992). Ancient plants were buried and turned into peat which is the precursor of coal. With burial, the peat was subjected to high temperature and pressure so it underwent coalification process to form mainly four types of coal: lignite, sub-bituminous, bituminous and anthracite. The higher the rank is, the higher the degree of coalification is.

2.1.2 Physical Structure of Coal

Coal is generally thought to have dual-porosity system consisting of a microporous matrix and macro-porous fractures (Van Krevelin, 1993). Micro-pores are the pores less than 2nm in size and more than 95% of gas in adsorbed phase are stored in them. Macro-porous fractures called the cleat system serve as the main pathways for gas to pass, so it is an important factor in determining the permeability. Cleat are fractures that typically occur at two sets which are normally perpendicular to the bedding planes and typically mutually orthogonal. Through-going cleats were firstly formed, which are called face cleats. The cleats form later and end within the intersections of face cleats are called butt cleats (Laubach & Tremain, 1991; Kulander & Dean, 1993).The cleat system provides a physical network for the fluid, gas and formation water, to flow through the formation towards the wellbore with pressure driven force during the production. The cleat system is passively changed with the gas depletion or injection. Quantification of these structural changes is challenging since it was determined by multiple chemiphysical processes.

2.1.3 Gas Storage in CBM Reservoirs

Methane is stored in coal in three types, gas adsorbed on the surface of micro-pores, free gas in the pores or fractures and gas dissolved in the water in coal seam (Rightmire et al. 1984). Actually, about 95% of the methane in the coal seam is of absorbed state. Therefore, compared with the natural gas in conventional reservoir, such as sandstone reservoir, coalbed methane reservoir could store much larger amount of gas due to the adsorption on the internal surface of pores.

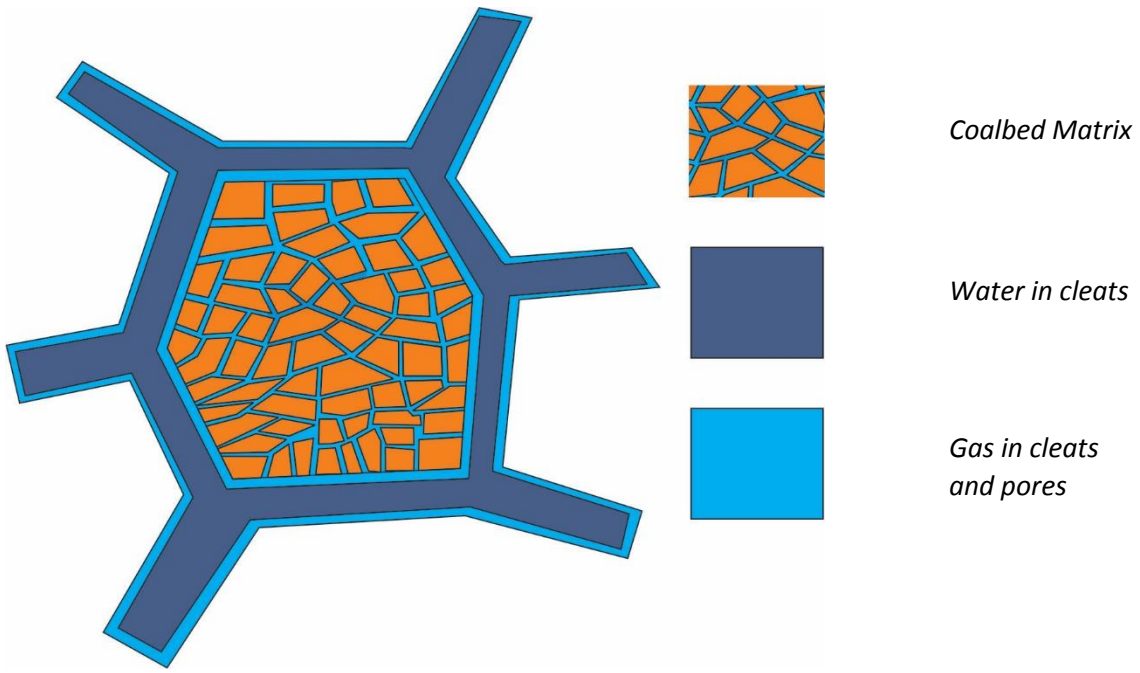

Figure 2.1: Illustration of coal matrix

Adsorption is a process in which gas molecules adhere to a surface, thereby forming a monolayer or multilayer film (Pashin, 2008). A monolayer is a film with the thickness of one molecule, whereas a multilayer is a film with a thickness of two or more molecules. Adsorption is thought to be a response to a natural bonding deficiency that exists along the surface. There are two kinds of adsorption: chemisorption and physisorption. Physisorption is adsorption by Van der Waals force, which is a weak intermolecular force and can result in the development of a monolayer or multilayer film. In general, physisorption is considered to be the dominant mode of sorption for gas in coal, although most workers consider monolayer adsorption to predominate because of the limits space in coal nano-pores (Pashin, 2008).

For coal, the adsorption process is directly affected by pressure, temperature, coal rank, mineral, element content, moisture, lithological properties and gas composition (Levy, et al.,

1997). Therefore, the amount of adsorption of a specified gas on a specified coal is a function of temperature and pressure (Yang, 1987):

$$V = F(P, T) \tag{2-1}$$

When the temperature is constant, the amount of adsorption is only a function of pressure. The typical sorption isotherm is a relationship between the amount of gas adsorbed and the pressure at a constant temperature.

The most popular method for adsorption is the Langmuir isotherm developed by Langmuir (1918). In his research, mica, glass and platinum were used to adsorb gas. A semi-empirical isotherm with kinetic basis was derived based on the experimental data. The equation is based on the assumptions that the equilibrium of adsorption reaches when the rate of adsorption or condensation equals to the rate of desorption or evaporation and that each site can only be occupied by one atom or molecule.

The rate of adsorption per unit area can be expressed as:

$$R_a = av(1 - \theta) \tag{2-2}$$

where, a represents the sticking probability, v is the collision frequency of the molecules or atoms striking the surface, and θ is the percentage of surface area which has been occupied by absorbate.

The collision frequency of molecules striking a solid surface can be expressed as:

$$v = \frac{p}{\sqrt{(2\pi M \kappa T)}} \tag{2-3}$$

The rate of desorption can be expressed as:

$$R_d = \beta\theta e^{-\mathrm{E}_d/RT} \tag{2-4}$$

where, β is the rate constant of desorption, E^d is the activation energy of desorption and R is the gas constant.

The rate of desorption equals the rate of adsorption when the system gets equilibrium:

$$\beta\theta e^{-\mathrm{E}_d/RT} = a \ \frac{p}{\sqrt{(2\pi M\kappa T)}}(1-\theta) \tag{2-5}$$

Through rearrangement,

$$\theta = \frac{BP}{1+BP} \tag{2-6}$$

Where $B = \frac{a}{\beta\sqrt{(2\pi M\kappa T)}} e^{-E_d/RT}$ is named Langmuir constant, P is the pressure and θ is the percentage of surface area occupied by absorbate.

Other than Langmuir isotherm, some other models have been derived. Brunauer, Emmett and Teller (1938) came up with a model applied to multilayer adsorption and aimed to explain the physical adsorption of gas molecules on solid. This kind of model is suitable for the strong adsorption. Polanyi (1963) proposed the potential theory of adsorption.

2.1.4 Gas Transport in Coalbed Reservoir

Gas transport process in coal matrix, from micro-scale to macro-scale, can be divided into three stages: desorption from the internal surface of coal; diffusion (Fick's law) from matrix to cleats; laminar flow (Darcy's Law) from cleats to production wells. Figure 2.2 shows each

mechanism schematically.

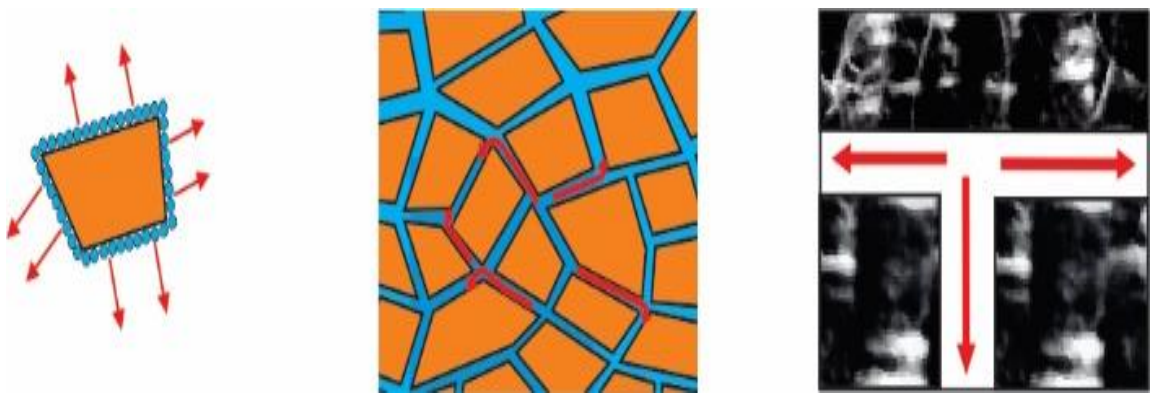

(a) (b) (c)

Figure 2.2: Transport mechanism: (a) Desorption from internal surface of micro-pores; (b) diffusion in matrix; (c) Laminar flow in cleats

Desorption is the phenomenon that gas molecules detach from the internal surface of coal matrix. When the pressure of reservoir is reduced, the process of desorption is initiated and the content of free gas increases.

Diffusion is the movement of atoms from a region of high concentration to a region of low concentration. Depending on the coal structure and pressure, one or more in Knudsen, bulk, and surface diffusions could happen in coal matrix (Smith and Williams, 1984). The process of diffusion is described in Fick's law, which is given as:

$$m=-D\nabla C \tag{2-7}$$

where, m is the mass flowrate, D is the diffusion coefficient, and ∇C is the magnitude of the concentration gradient.

Darcy's flow is found to be the flow mechanism in cleats and fractures which are main pathway during CBM production. Besides CBM, water exists in the flow system during production as well.

2.2 Fundamentals of Marcellus Shale

With advances in drilling and completion technology, especially horizontal drilling and hydraulic fracturing, the production of shale gas has gained significantly commercial success (Hao et al., 2013). The shale has been known for years as reservoir source rock, but it was only recently considered as valuable reservoir rock due to the state-of-the-art drilling and completion technologies. However, the challenge of shale gas development is the lack of comprehensive understanding of the fluid dynamics in the ultra-tight pore micro-structure. Over the last several years, significant effort has been made on gas shale reservoir characterization. However, there are still some untouched areas due to the complexitiy of the shale composition. As the shale gas industry proceeds, the characteristics of shale as a petroleum source rock is required to be better understood in order to improve the production.

2.2.1 Shale Rock Origin and Composition

Shale is a kind of sedimentary rock typically formed by compaction in very slow moving water at certain temperature and pressure. Therefore, it is often found in lakes deposits, in river deltas, sedimentary basin or continental shelf. Shale is usually composed of variable amount of clay minerals, organic matter and other minerals such as quartz, feldspar or calcite. Dependent on the compositions, shale could be of several types such as oil shale, grey shale, and black shale and so on. Within those kinds of shale, oil shale and black shale are thought to be rich in organic matter. Oil shale contains organic matter in the form of kerogen up to 1/3 of the rock. The

Marcellus shale is black shale with organic matter ranging from 1% in eastern New York to over 11% in the central part of the state (Nyahay et al., 2007).

2.2.2 Shale Rock Pore Structure

The pores in shale are classified as micro-pores (<2nm), meso-pores (2~50nm) and macro-pores (>50 nm). Aggregates of kerogen, Clay and carbonate contain most of the macro-pores and meso-pores. With the decrease of porosity, micro-pore volumes relatively increase whereas the sum of meso-pore and macro-pore volumes decrease (Chalmers et al. 2012).

The gas shale in US is clay and quartz rich. Macro-pores and meso-pores are observed as inter-granular porosity or confined to kerogen rich aggregates(Chalmers et al. 2012).

2.2.3 Gas Storage in Shale Reservoir

Due to the properties of black shale, it could serve as overlaying formation of petroleum source rock to store the conventional gas, as unconventional gas reservoir and as underlying formation to seal the petroleum. The gas storage in shale is almost the same as coal. The gas could be stored as free gas in natural fracture or inter-granular porosity, as gas adsorbed onto the surfaces of organic matter or clay minerals, or as dissolved gas in oil and water (Curtis, 2002).

2.2.4 Gas Transport in Shale Reservoir

Two different sized porous media, i.e., organic and inorganic, are revealed in organic-rich shale. Each porous medium has its own transport mechanism. Inorganic pore is relatively large. Gas transport is viscous force controlled flow which is usually treated using Darcy's law in the reservoir. Gas Transport in organic matter is complex. Due to the sizes of organic pores, some non-Darcian effects could be included. For pore with size above 100nm, Darcy's law could be

valid. For smaller pore, however, gas transport is caused by the slippage mechanism of free gas and hopping mechanism of the absorbed gas molecules (Akkutlu & Fathi, 2011). When the pore size is approaching nano-scale, the gas transport is even more complex that may involve molecular-pore wall interactions and Knudsen diffusion and surface diffusion will be dominant the mass transfer process. In addition to these complex flow regimes, the pore structure is known to be no long keep constant during the gas flows since the scale of the structural changes might be in the same order as the pore size which will be significantly influence the flow behavior. This structure change is not obvious and negligible for the conventional reservoirs because the scale of these change is of a few order of magnitude smaller than the pore size dimensions.

CHAPTER 3

LITERATURE REVIEW

The swelling and shrinkage behaviors of sorptive rocks are important for reservoir engineers to interpret the variation of production and predict the production in the future. Gas sorption-induced coal deformation has been studied for more than sixty years by various researchers. A lot of experimental and theoretical results regarding to the coal shrinkage and swelling have been reported and discussed in the open literature. With the commercialization of shale gas industry, the sorption-induced shale matrix deformation becomes a potential root cause for the complex fluid flow dynamics. However, very limited efforts have been devoted on characterizing shale shrinkage and swelling due to some of the technical challenges. In this chapter, I conducted a literature survey on the sorption induced shale and coal matrix deformations.

3.1 Experimental Investigations of the Coal and Shale Matrix deformations

3.1.1 Shrinkage and Swelling of Coal

Moffat and Weale (1955) were the first to report a volumetric strain of coal block with rank ranging from low volatile to semi-anthracite, when subjected to methane pressure as much as approximately 15 MPa. Whereas, when the pressure is between 15 MPa and 71 MPa, the volume of coal block will no longer increase. Instead, it decreases or remains constant. That is due to the solid volume and the grain compressibility effect.

Harpalani and Schraufnagel (1990) measured the volumetric strain of coal matrix for two cycles: helium and methane. They found that for helium, with the increasing of the pressure,

volume of the coal shrinks linearly; by contrast, volume of the coal swells linearly with the decrease of the pressure, but it cannot come back to zero because the coal is not perfectly elastic. For methane, at 6.9 MPa, the volume of the coal increased by about 0.5%. At atmospheric pressure, the volume of the specimen remained 0.1% which is higher than its original value. They thought it may be caused by the residual gas or the short of time.

Seidle and Huitt (1995) concluded the results of several previous researchers and said the shrinkage coefficients were in the range of 1 to 10 E-6 PSI-1. Also, an experimental apparatus was assembled to measure the coal matrix swelling. In the experiment, a San Juan basin coal sample was subjected to methane up to 2000 psi, followed by helium cycle up to 2000 psi. Finally carbon dioxide cycle up to 900 psi was injected. The swelling coefficients of 0.86 us-ton/scf and 0.78 us-ton/scf were obtained separately by using methane and carbon dioxide.

Levine (1996) proposed a langmuir-type equation which is $\varepsilon_s = \varepsilon_{max}.p/(p + p_{50})$ where ε_s is the linear sorption strain at pressure P. ε_{max} is representative of the theoretical maximum strain. P_{50} is the pressure at which the coal has attained 50% of its maximum strain. And it also shows that significant changes in permeability could occur during gas production due to matrix shrinkage, but the rank, petrographic composition, mineral matter content and sorbate composition are all significant in controlling the magnitude of the effect.

Harpalani and Chen (1997) designed an experimental technique to separate the effects of effective stress, gas slippage, and matrix shrinkage on permeability of coal and they found that the effect of gas slippage is relatively small compared to the effect of matrix shrinkage for gas pressure above 1.7 Mpa. In contrast, below 1.7Mpa, both gas slippage and matrix shrinkage effects are important of determining the permeability. They also concluded that the change in

permeability resulting from matrix shrinkage is linearly dependent on the amount of gas desorbed.

Georage and Barakat (2001) measured the volumetric strain of coal sample from the ohai coal mine in the south island of New Zealand. At about 4mpa, the volumetric strain for Carbon Dioxite is about 2.2% which is 12 times higher than nitrogen and eight times higher than methane.

Majewska and Zietek (2006) measured the strain change on medium-rank coal subjected to three successive cycles of sorption-desorption processes of a single gas. They found the anisotropy in swelling/shrinkage exists in each cycle.

Harpalani and Mitra (2010) conducted an experiment to test 2 kinds of sample which are from San Juan and Illinois respectively. For pressure up to 5.5 Mpa, the volumetric strain of Illinois core is 0.58% with methane and 2.0% with CO_2. For San Juan Coal at 5.5Mpa, the volumetric strain is 0.6% with methane and 1.2% with carbon dioxite.

Sakurovs (2011) compared the high and low pressure sorption behavior of 28 bituminous and subbituminous coals for carbon dioxide and found that the sorption capacity calculated from high pressure sorption was always greater than that calculated from low pressure. The difference between sorption capacities from low pressure to high pressure increased with decreasing ranks. This phenomenon was explained qualitatively by swelling of the coal in high pressure that does not occur in low pressure condition.

Day et al. (2012) reported laboratory measurements of swelling in four Australian bituminous and sub bituminous coal in CO_2, methane and the mixed gas. The volumetric strain at 15MPa ranged from about 1.9 % to 5.5% in CO_2 and 1.0% to 2.5% in CH_4. The experiment

shows there is no enhanced swelling in mixed gases compared with the pure CO_2 at the same total pressure.

Majewska et al. (2013) measured the swelling of cylindrical coal sample by CO_2 sorption in unconfined condition and axial compressed condition respectively. The results showed that the swelling reduced by about 60% in axial compressed condition, which might imply the self-stressing as a result of CO_2 sorption by coal under constrained condition.

Liu and Harpalani (2013) measured subbituminous coal samples from San Juan Basin. The samples were subjected to increasing methane pressure in a stepwise manner of 1.4 MPa to a 4final pressure of 7 MPa. The Volumetric Strain was calculated from the sum of strains of three directions. The data were fitted perfectly with Langmuir-type equation.

Staib et al. (2014) measured kinetics of coal swelling of five Australian bituminous coals in the environment of CO_2, CH_4, Xe and ethane. The Swelling rate was found to depend on gas type. In the comparison between CO_2 and CH_4, CH_4 was found to swell slowly than CO_2 at same pressure. Besides, the composition of coal affects the swelling rate also. The vitrinite-rich coal was found to swell slower. With the increasing of pressure, the swelling rate is increasing in slowest swelling coal, and for fastest swelling coal, the swelling rate shows a decreasing trend at relatively higher pressure.

Anggara et al. (2014) measured two group of samples of Miocene low rank coal with different megascopic textures to see the different swelling behaviors of them. Banded coal tends to have higher amount of suberinite and corpohuminite maceral, and non-banded coal, in contrast, tends to have lower such materials. The samples are measured in free standing status. The swelling of banded coal is anisotropic while that of non-banded coal is isotropic. The

conclusion that megascopic textures control the swelling behavior with respect to bedding orientation was made.

Zang et al. (2015) regressed the internal swelling which means the swelling of cleats, from a proposed permeability model. The results showed that the internal swelling was positively proportional to pore pressure and negatively to confining stress for methane and gaseous carbon dioxide, but for supercritical carbon dioxide, the confining stress was not the determinant factor and pore pressure had same effect on internal swelling. The internal swelling ratio which means the ratio of internal swelling to gas- induced swelling of coal matrix or coal block was found to be nearly constant during coalbed methane production when the in-situ stress was greater than 5MPa.

3.1.2 Shrinkage and Swelling of Shale Matrix

Because of the technical challenges, the shale matrix deformation is very small and the measurement resolution has to be small enough to detect the deformation. Liu (2014, personal communication) has tried to apply the strain-gauge-based method to measure the strain, but the results were very noisy and negligible. The reason was attributed to the strain-gauge does not have the resolution.

Heller and Zoback (2014) presented an experimental study on the shale matrix sorption induced shrinkage and swelling by using powder-based shale briquette. They measured methane and carbon dioxide adsorption isotherms on the carbon and clay samples and the results are all fitted with Langmuir isotherm model very well and carbon dioxide is approximately 2-3 times the adsorptive capacity of methane and the amount of swelling is approximately linearly

proportional to the amount of adsorption. The magnitude of swelling of carbon and clay minerals is on the range from 10^{-5} to 10^{-3}.

Based on the description (Heller and Zoback, 2014; Liu, 2014), the measurement of such deformation of shale is challenging due to two reasons. First, it takes very long time for an intact shale core sample to swell. Second, the amount of adsorption of gas shale is measured to be an order of magnitude less than that of coal. Assume the adsorption-induced strain is positively proportional to amount of adsorption, the magnitude of swelling /shrinkage of shale is almost an order less than that of coal. Such small strain is hard to measure using traditional method.

3.2 Theoretical Modeling of Sorption-induced Coal and Shale Deformation

Pan and Connell (2007) derived a theoretical model to describe adsorption- induced coal swelling at adsorption and strain equilibrium. This model is based on the energy balance approach, which assumes the surface energy change due to adsorption is equal to the elastic energy change of the coal solid. The parameters, such as elastic modulus, gas adsorption isotherm, coal density and porosity are required in the model.

The eventually formula combining adsorption and compression strain:

$$\varepsilon = -\frac{\phi\rho_s}{E_S} f(x, v_s) - \frac{P}{E_S}(1 - 2v_s) \tag{3-1}$$

where, ϕ is the surface potential of sorption, ρ_s is the density of the solid adsorbent, E_S is the Young's modulus of the solid absorbent, P is the pressure, v_s is the Poisson's ratio.

$$f(x, v_s) = \frac{[2(1-v_s)-(1+v_s)cx][3-5v_s-4(1-2v_s)cx]}{(3-5v_s)(2-3cx)} \tag{3-2}$$

where c=1.2, v_s is the Poisson's ratio, x=a/l, a and l are the cylindrical radius and length of certain pore structure model.

This theoretical model can represent the differential swelling behavior based on gas type. Furthermore, this model could describe the swelling behavior caused by mixed gas adsorption.

Liu and Harpalani (2013) proposed a new theoretical model based on the theory of changes in surface energy as a result of sorption. In the model, the total strain is divided into sorption-induced strain and mechanical strain. The theory of Bangham and Fakhoury (1931) is used to derive the sorption-induced strain:

$$\varepsilon_a = \frac{3a\rho RT}{E_A V_0}\int_0^P \frac{b}{1+bp}dp \tag{3-3}$$

where a and b are Langmuir constants, ρ is coal solid-phase density, R is universal gas constant, T is temperature, E_A is modulus of solid expansion resulting from adsorption and desorption , V_0 is gas molar volume.

Mechanical strain caused by stress or pressure alone is given as

$$\varepsilon_m = -\frac{3P_S}{E}(1-2v) \tag{3-4}$$

where P_s is the stress experienced by solid, E is the young's modulus, v is the Poisson's ratio.

The overall volumetric strain can be expressed as given

$$\varepsilon = \varepsilon_a + \varepsilon_m = \frac{3a\rho RT}{E_A V_0}\int_0^P \frac{b}{1+bp}dp - -\frac{3P_S}{E}(1-2v) \tag{3-5}$$

The results shows that the proposed model could fit the experimental data in the literatures in the past 50 years very well.

To my best knowledge, no model has been proposed to describe the sorption induced shale matrix deformation.

CHAPTER 4

DEVELOPMENT OF A NEW OPTICAL STRAIN MEASUREMENT APPARATUS

Many experiments about sorption-induced strain for coal have been conducted since this strain is directly related to poroelastic responses with gas depletion. However, most of measurements were done on large coal bulk. For shale, there is no publication about sorption-induced swelling/shrinkage on intact shale matrix to date. In order to thoroughly understand the deformation of sorptive rock matrix (coal and shale) subjected to different gases (helium, methane and carbon dioxide), a high resolution strain measurement system was established with High-Resolution Optical Microscope to quantify the deformation of millimetre-sized samples directly. The tested resolution is about 2 microns.

4.1 Establishment of Optical-Based Experimental Apparatus

The initial idea was to measure the linear strain based on the displacement between two pin-points on the surface of an object using high-resolution microscope with gas injection. However, after a few trial runs, it was almost impossible to lock the pin-points when the sample was under deformation mode with gas injection. After consulting with the image processing experts, a final solution was established to quantify the areal strain of the tested samples. Figure 4.1 shows the layout of the experimental system which is consisted of a high-resolution optical microscope, a high pressure cell, computer and gas injection system.

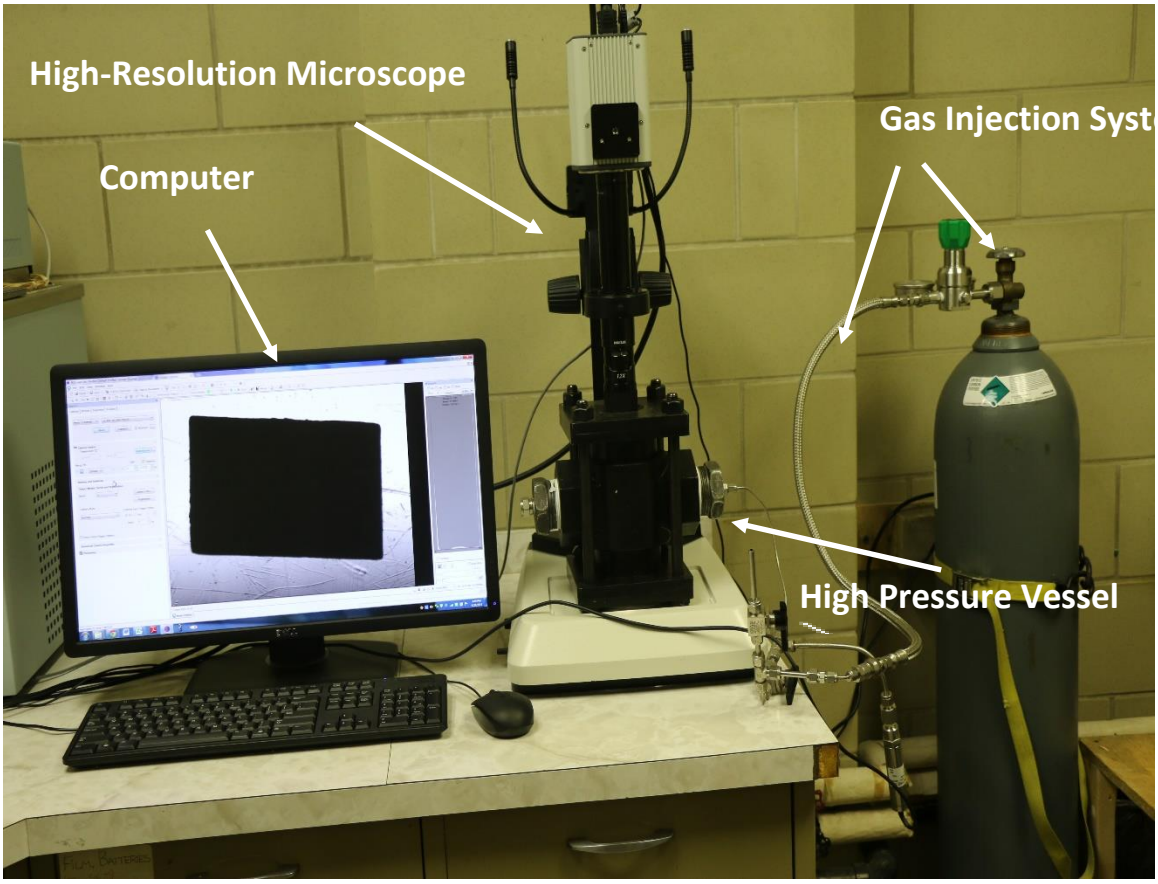

Figure 4.1: Layout of experimental system for strain measurement

The key component in this system is the high pressure vessel with two transparent windows which allow the direct observation of the deformation during gas injection through the high resolution microscope. The pressure vessel was customized. Each transparent window includes two layers of high strength glass. The vessel can sustain the gas pressure up to 13.79 MPa. Figure 4.2 shows the high pressure glass windows on the top and bottom which are identical. Figure 4.3 shows the side view of the vessel with the sample jack. The sample jack was customized by the machine shop and it can raise the sample at any level within the vessel. The schematic of whole vessel is illustrated in figure 4.4.

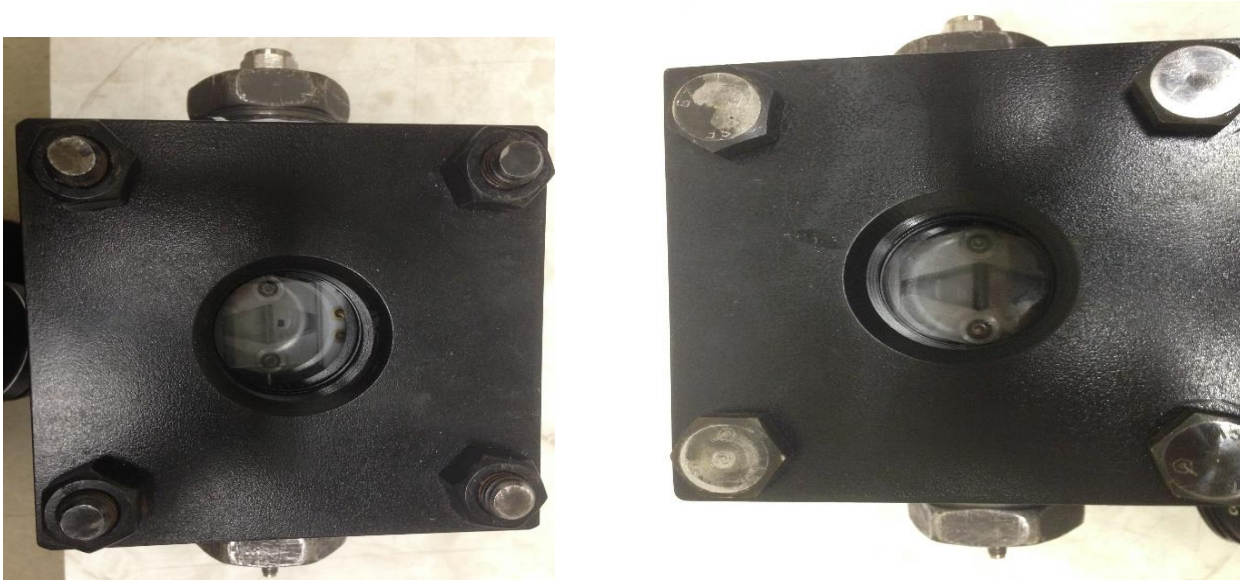

(a) (b)

Figure 4.2: (a) Top view of vessel; (b) Bottom view of vessel

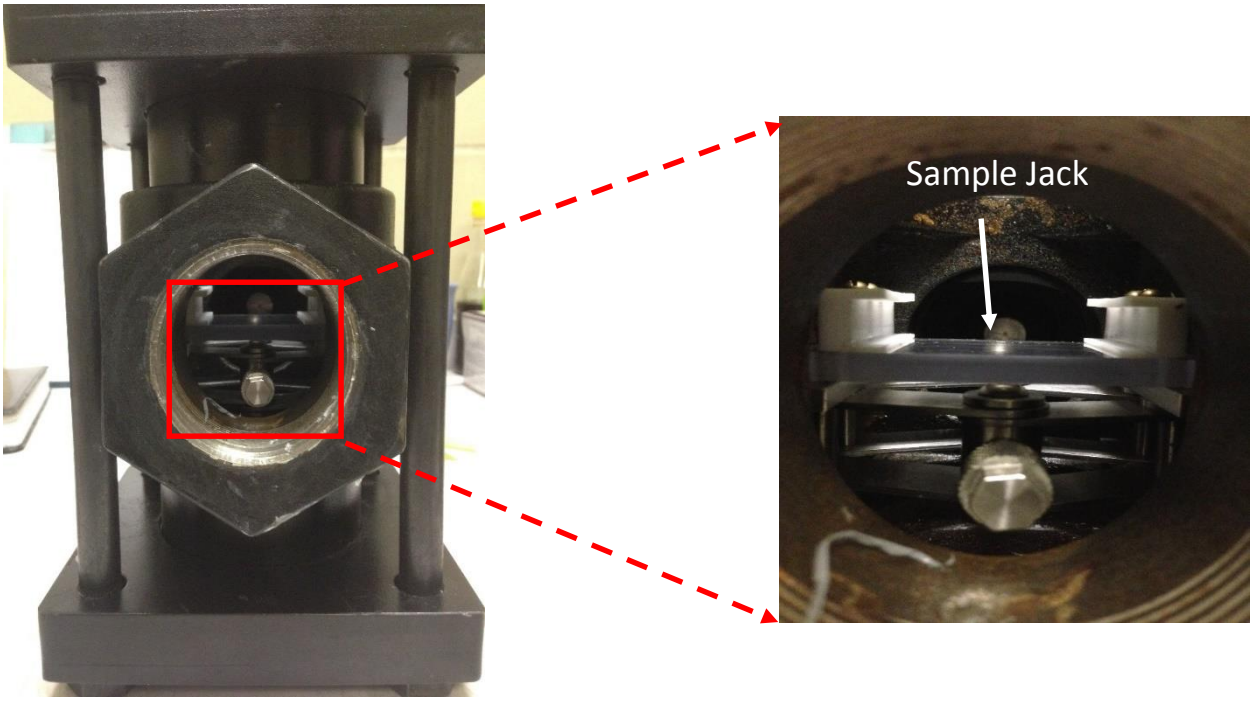

Figure 4.3: Side view of vessel with the sample jack.

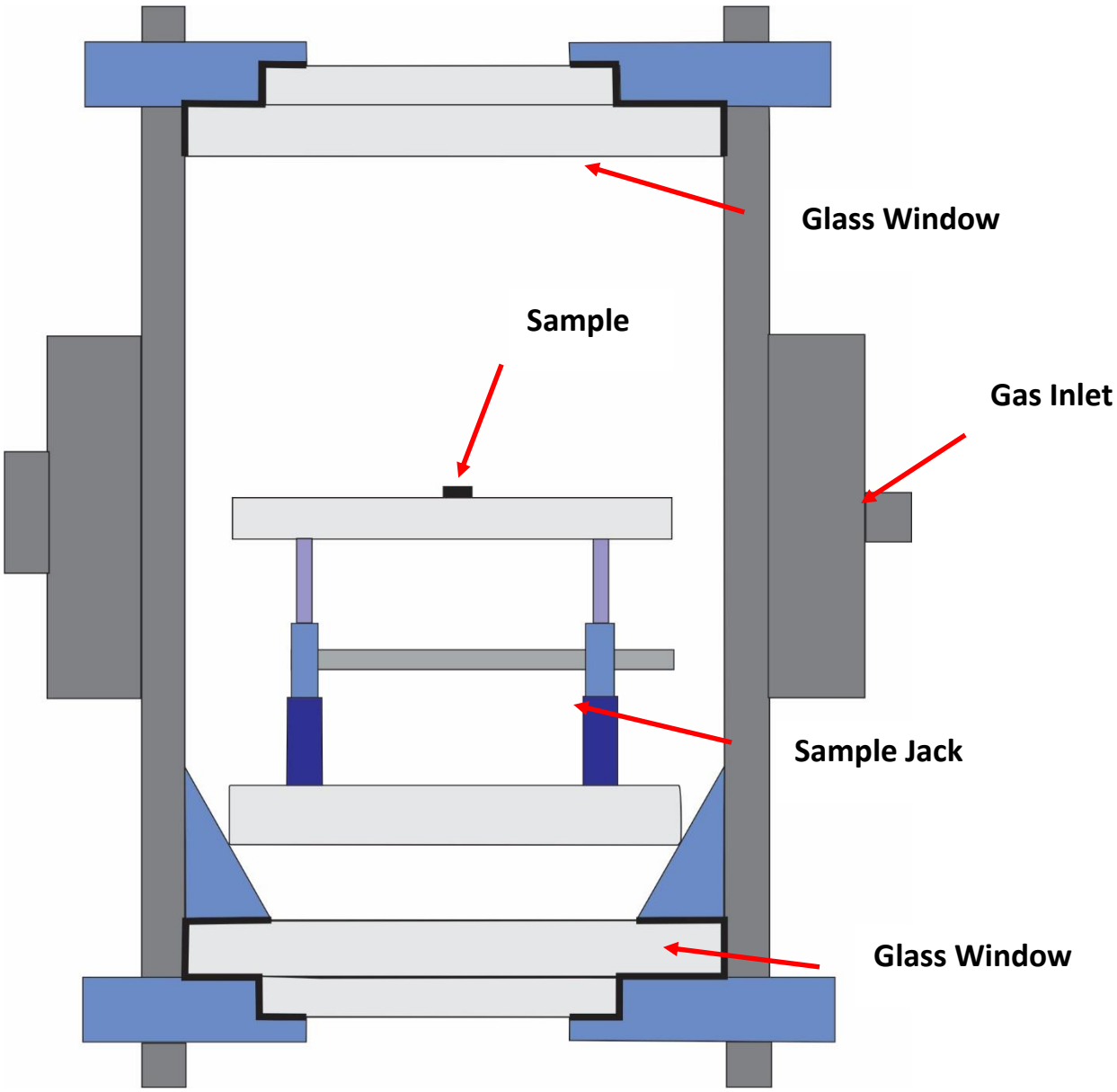

Figure 4.4: Schematic of vessel

In the optical measurement, for sake of the accurate quantification, the effects of the change of volume and the displacement of location need to be taken into consideration during the strain mapping. Therefore, the choice of lens is of great significance. In the experiment, Navitar's 12x telecentric lens was selected and being used. The actually lens was showed in figure 4.5.

Figure 4.5: Navitar's 12X telecentric lens

Telecentric lens has two advantages over conventional lens. Firstly, telecentric lens view the object in a "straight on" manner across the entire field of view, which makes images undistorted and features easy to examine. Conventional lens, in contrast, view the objects at different angle, making images distorted and features difficult to examine. Figure 4.6 shows the difference of images for this reason. Secondly, the magnification of telecentric lens is independent of working distance. Conventional lens, however, view objects that are closer to camera as larger than objects that are farther away. Figure 4.7 shows the difference of images for that reason.

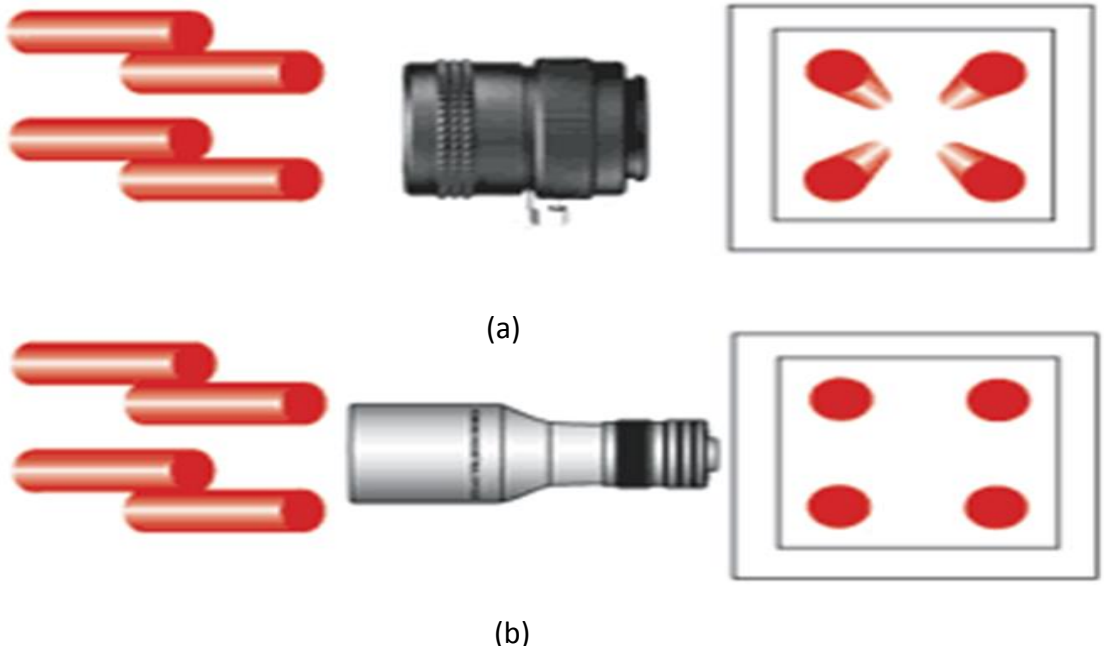

Figure 4.6: Comparison of perspectives in (a) conventional lens; and (b) telecentric lens (Navitar, 2013)

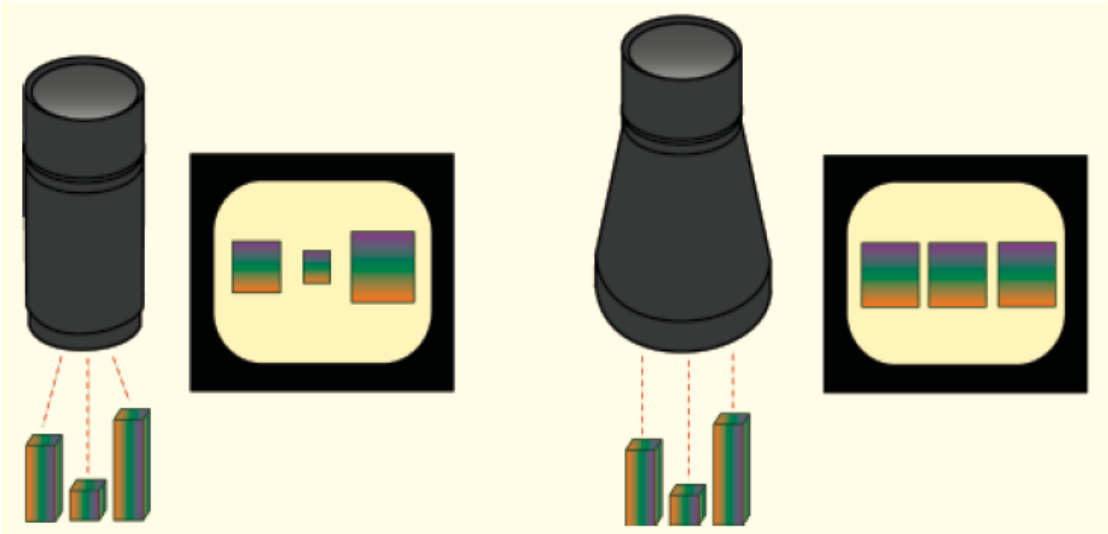

Figure 4.7: Comparison of magnification with different working distances in (a) conventional lens and (b) telecentric lens (Navitar, 2013)

In the current study, the angles of measurement might change due to the swelling or shrinkage of sample and slight displacements caused by turbulent induced forces of gas injection. Conventional lens is inaccurate because dynamic strain mapping is difficult when images are distorted and sample boundaries blurry. Telecentric lens, however, have satisfied quantification of strain with undistorted images and clear sample boundaries.

Swelling/shrinkage happens not only horizontally but also vertically which will increase or decrease the sample thickness. The magnification of Conventional lens would change with distance between sample and camera, which will give uncertainties of the strain mapping. However, telecentric lens's magnification is independent of working distance, which reduces the inaccuracy regarding magnification.

4.2 Experimental Specimen Preparation

Three specimens, two coal and one shale, were prepared. One bituminous coal was obtained from northern San Juan basin. The San Juan coal mine is located 25 kilometers west of Farmington, New Mexico. San Juan coal is bituminous coal which is relatively soft. As showed in figure 4.8(a), San Juan Coal is dark brown. The "bright, dull banded" feature could be observed clearly.

The second coal sample is an anthraciute coal which was collected from Hazleton in Pennsylvania. Anthracite coal is a hard, compact coal with high luster which can be seen in figure 4.8(c). The carbon content is highest and impurity lowest among all types of coal.

Figure 4.8(b) shows the shale sample collected from the deep Marcellus shale formation. All collected sample blocks were preserved at proper temperature and humidity conditions.

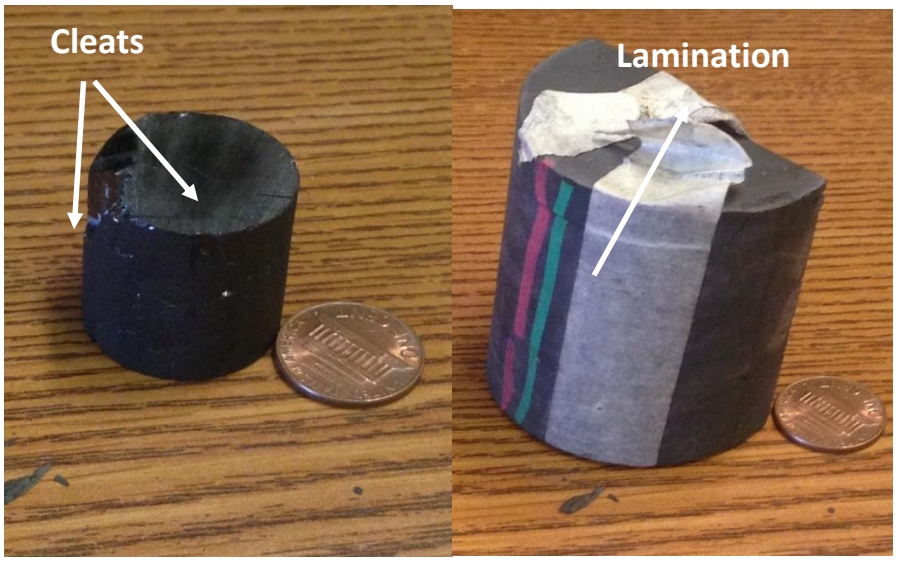

(a) (b)

(c)

Figure 4.8: (a) Core of coal from San Juan basin; (b) Core of shale from Marcellus formation; (c) Block of coal from Hazleton coal mine.

In this study, the specimens should be carefully prepared. Two requirements are needed to ensure the subsequent accurate imaging. First, all the specimens should have very clear boundaries, which means the sides of the specimen need to be perpendicular to the top and

bottom surfaces. Second, the thickness needs to be uniform and less than 2 mm if possible. Additionally, the specimen without the fracture or cleat was preferable so the size of samples need to be small enough that is less than the fracture/cleat spacing. In this study, the specimens with dimension of ~3×3 millimeters were prepared. Besides, the coal and shale samples are both very fragile, so they cannot be handled by standard high speed cutoff machines. Based on the need of precise cutting and fragileness of coal and shale, a set of slow-speed saws are used to get high quality surfaces. Figure 4.9 shows the set of slow-speed saws with different cutting precision.

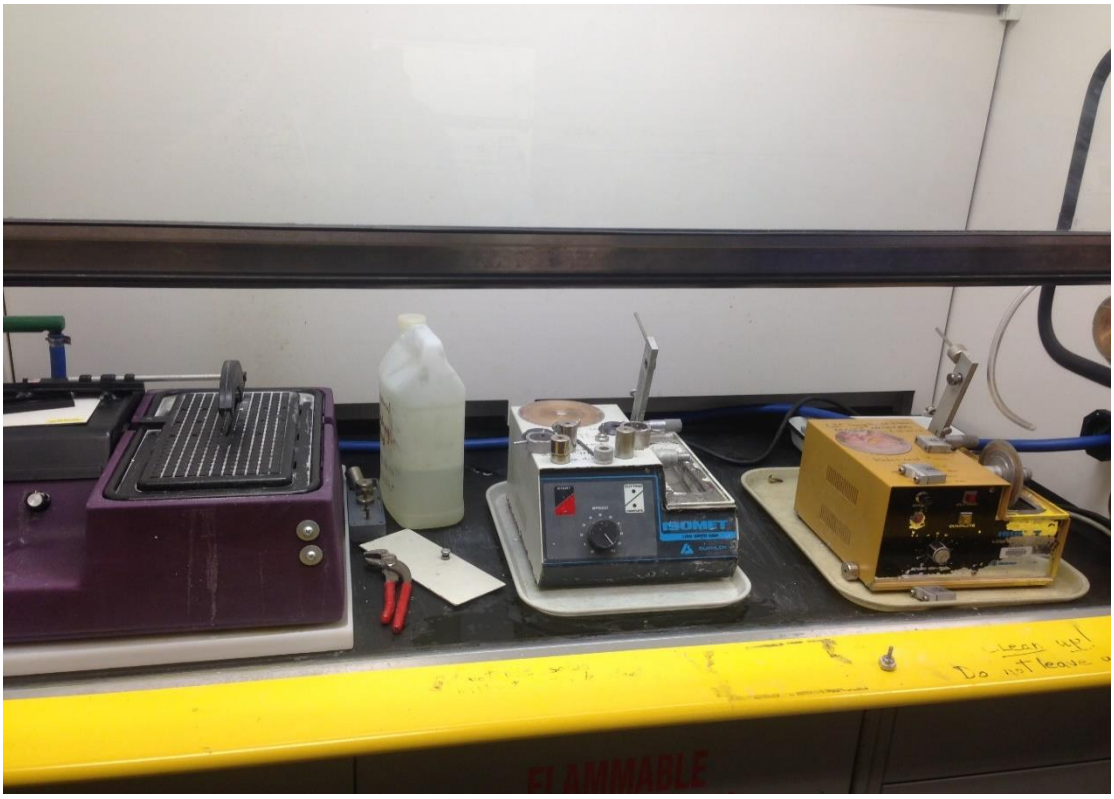

Figure 4.9: Slow-speed saws with different cutting precision

Figure 4.10 shows the well-prepared specimens of San Juan coal and Marcellus shale. Their size, thickness and shape are made suitably for imaging.

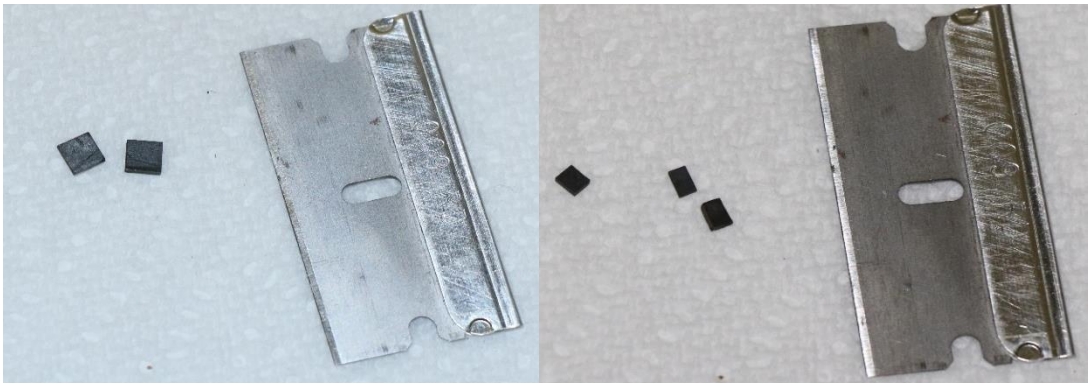

(a) (b)

Figure 4.10: (a) Specimens of San Juan coal; (b) Specimens of Marcellus shale

4.3 Experimental Work on Strain Mapping

4.3.1 Initial Test -One

An initial test was designed to test the possibility of measuring sorption-induced strain using the established optically-based experimental system. For this experiment, CO_2 was used as sorbing gas and Helium as non-sorbing gas. Because this trial test was done before the preparation of square specimens, a relatively thick sample with irregular shape was used during the measurement. Gooseneck lights were used in order to define two pin-points in the surface of coal and see the dynamic deformation. In this way, we can observe and calculate the linear strain directly. Figure 4.11 shows the gooseneck lights. At 75°F, the strain of 0.08% in 0.69 MPa CO_2 and -0.15 % in 1.38 MPa helium was observed and estimated. The results showed that measurement of strain using optical method was possible and practical.

Although the deformation was observed on the tested coal sample, the locations of the two pin-points are extremely hard to fix at different injection pressures. The reason is that the camera captures the reflect light from the pin-points and it might change along with the

deformation. The uncertainty will give errors on the linear strain calculation. In order to eliminate the uncertainty, a second trial test based on the area strain theory was designed and conducted. The details were presented in the next section.

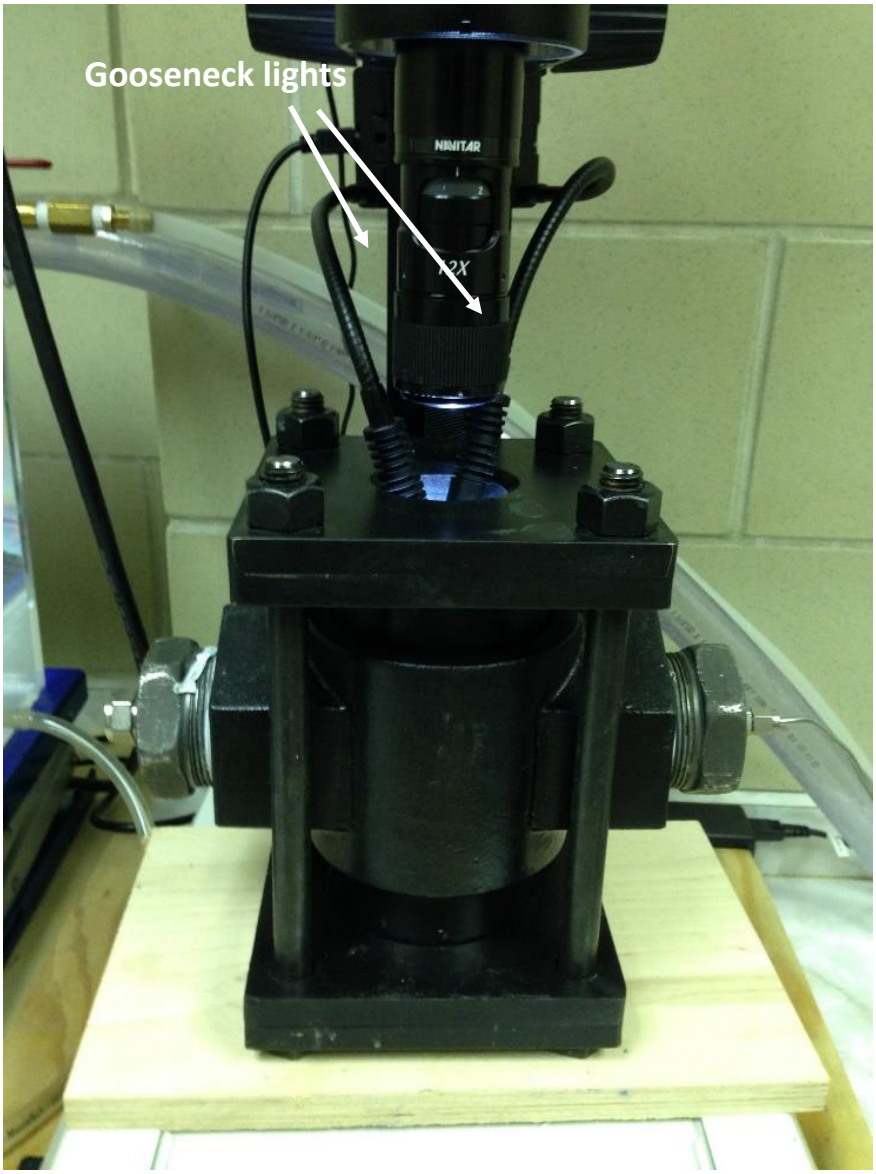

Figure 4.11: Layout of gooseneck lights

4.3.2 Initial Test-Two

After considering the difficulty of locking single pin-point, area strain of specimen was measured using gooseneck lighting. Some extent of deformation was detected with pressure increase. However, the boundaries of the specimen were blurry in the images, which would increase the errors. In order to reduce image blur, gooseneck lighting was thought to be unsuitable for this experiment.

4.3.3 Final Experimental Plan

Finally, gooseneck lights were replaced by backlight illumination. In this way, the boundaries became extremely clear with the cuboid specimens. After satisfaction of precision and proof of feasibility, the official experiment was conducted as follows:

Experimental Procedure

The first step of the experiment was to place the specimen in the pressure vessel at the location where entire sample could be clearly seen by the microscope. Then, camera was adjusted until the screen was filled with the sample properly. Then the pressure cell was sealed by installing the sealant and gasket seal sets. Following this, helium at 0.69 MPa was injected and ejected three times to remove the residual air within the vessel. In this experiment, three times injection and ejection of tested gas was thought to well replace residual gas with tested gas. At the last step of helium flushing, the pressure cell was tested for the leakage-proof by using Swagelok leakage tester. The cell was properly seal. Upon this point, the experiment can be initiated.

The experiment was completed by dosing coal or shale specimen with helium in a step of 0.69-1.72 MPa to a final pressure of 6.89 MPa. After each injection, plane strain was monitored

by capturing images continuously till sample achieved equilibrium. Because the specimen was extremely small in size, it could be considered in equilibrium if the strain remained stable for 1 hours. After a few trial and runs, 30 minutes were considered enough for the specimen to get mechanical equilibrium. For helium, known to be a non-sorbing gas, the measured shrinkage is purely due to the mechanical compression of the matrix of coal or shale.

After completion of the helium cycle, the vessel was flushed with carbon dioxide three times also in order to get rid of the residual helium gas. The sample was then saturated with carbon dioxide up to around 5.17 MPa with the steps of 0.69-1.38 MPa. The strain did not have big change after 2 days, so 2 days were thought to be enough for adsorption equilibrium. After finishing each injection and achieving new pressure, the extra operation of refocusing was necessary to counteract the swelling in the vertical direction. The microscope monitors the strain at each pressure to see the dynamic deformation of sorptive rock.

Image processing

During the image processing, the size of the specimen was computed by counting the number of pixels of the sample. Here, I will take carbon dioxide as an example. As the adsorption achieved equilibrium, 200 images were captured continuously. Figure 4.12 shows a single image collected for one specimen.

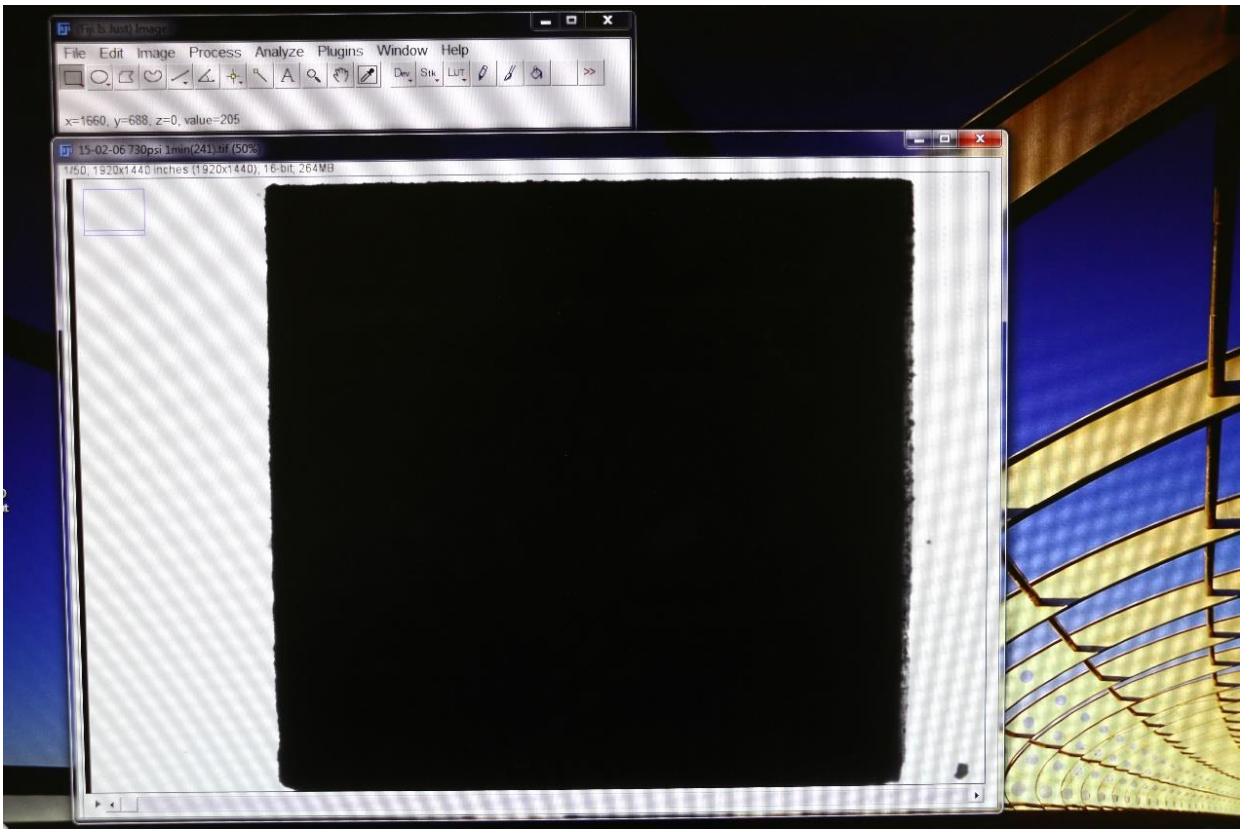

Figure 4.12: Images collected after equilibrium of adsorption for CO_2

After the acquisition of images. Fuji software was employed to do the subsequent image processing. The median intensity image was produced by stacking all of that and take the median average. Then, the threshold of the image was adjusted in a range where the sample could be distinguished from the background clearly. Now, only the pixels of sample remained in the image. The maximum number of pixels are 2173304, which means 1474 pixels linearly (one direction). The size of sample is 3 mm; therefore, the precision is about 2 microns. Figure 4.13 shows the median intensity image after adjusting threshold. Red area represented the sample area. The small spot in black circle was needed to be got rid of. Based on the number of pixels, the areal strain can be quantified by comparing the pixels before and after each pressure step.

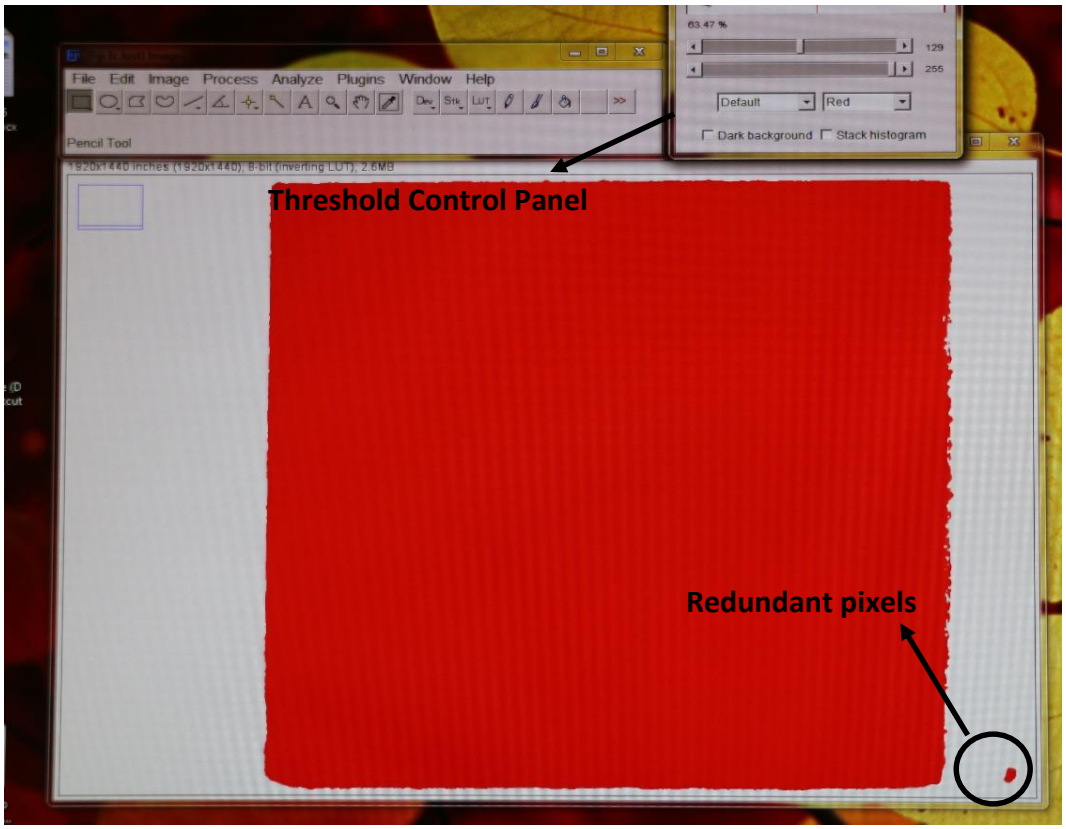

Figure 4.13: Median intensity image after adjusting threshold

4.3.4 Error in Image Processing

Although some modifications had made to reduce the errors what can be imagined. The error during imaging was unavoidable. In order to answer the question that whether the imaging error affected the results seriously or not, ten sets of images were taken continuously from one specimen. The median-intensity images were calculated from the sets. The standard error in imaging was 0.0000268, which was at least one order less in magnitude than the adsorption-induced strain. Therefore, the results were considered to be valid and trustful. Table 4-1 shows the calculation of standard error.

Time	Planar Area(Pixels^2)	Areal Strain
1	1720786	-0.000691067
2	1720687	-0.000748559
3	1720705	-0.000738106
4	1720657	-0.00076598
5	1720694	-0.000744494
6	1720656	-0.000766561
7	1720637	-0.000777595
8	1720621	-0.000786887
9	1720703	-0.000739267
10	1720672	-0.00075727
Mean:	1720681.8	-0.000751578
Standard Error:	46.0695127	2.67539E-05
	Original Area(Pixels^2)	
	1721976	

Table 4.1: Calculation of standard error in imaging

4.4 Relationship between Areal Strain and Volumetric Strain

An important reason for obtaining strain data is to relate the changes of permeability with strain data. Therefore, volumetric strain is more critical than areal or linear strain for modeling changes of permeability from industrial and practical view. A mathematical relationship between volumetric and areal strains was derived here.

The areal strain is defined as the change in the plane surface area of a sample divided by its original area:

$$\varepsilon_A = \frac{\Delta A}{A} \tag{4-1}$$

where, ΔA is the change of surface area and A is the original surface area.

The volumetric strain is defined as the change in volume of a sample divided by its original volume:

$$\varepsilon_V = \frac{\Delta V}{V} \tag{4-2}$$

where, ΔV is the change of volume and V is the original volume.

The linear strain is defined as change in length of a sample divided by its original length:

$$\varepsilon_L = \frac{\Delta L}{L} \tag{4-3}$$

where, ΔL is the change of length and L is the original length.

In this derivation, a simple rectangular model with L1 (Length), L2 (Width), and L3 (Height) is used. The change in volume (ΔV) could be expressed as

$$\Delta V = (L1 + \Delta L1)(L2 + \Delta L2)(L3 + \Delta L3) - L1L2L3 \tag{4-4}$$

Multiplying these terms and simplifying yields:

$$\Delta V = L2L3\Delta L1 + L1L3\Delta L2 + L1L2\Delta L3 + L1\Delta L2\Delta L3 + L2\Delta L1\Delta L3 + L3\Delta L1\Delta L2 + \Delta L1\Delta L2\Delta L3 \tag{4-5}$$

Volumetric Strain could be expressed as

$$\varepsilon_V = \frac{\Delta V}{V} = \frac{L2L3\Delta L1+L1L3\Delta L2+L1L2\Delta L3+L1\Delta L2\Delta L3+L2\Delta L1\Delta L3+L3\Delta L1\Delta L2+\Delta L1\Delta L2\Delta L3}{L1L2L3} = \frac{\Delta L1}{L1} + \frac{\Delta L2}{L2} + \frac{\Delta L3}{L3} + \frac{\Delta L2\Delta L3}{L2L3} + \frac{\Delta L1\Delta L3}{L1L3} + \frac{\Delta L1\Delta L2}{L1L2} + \frac{\Delta L1\Delta L2\Delta L3}{L1L2L3} = \varepsilon_{L1} + \varepsilon_{L2} + \varepsilon_{L3} + \varepsilon_{L2}\varepsilon_{L3} + \varepsilon_{L1}\varepsilon_{L3} + \varepsilon_{L1}\varepsilon_{L2} + \varepsilon_{L1}\varepsilon_{L2}\varepsilon_{L3} \tag{4-6}$$

Assuming L1, L2 are within the surface and L3 is perpendicular to the surface. Therefore, the change in surface area (ΔA) could be expressed as:

$$\Delta A = (L1 + \Delta L1)(L2 + \Delta L2) - L1L2 \tag{4-7}$$

Multiplying these terms and simplifying yields:

$$\Delta A = L2\Delta L1 + L1\Delta L2 + \Delta L1\Delta L2 \tag{4-8}$$

Areal strain could be expressed as:

$$\varepsilon_A = \frac{\Delta A}{A} = \frac{L2\Delta L1 + L1\Delta L2 + \Delta L1\Delta L2}{L1L2} = \frac{\Delta L1}{L1} + \frac{\Delta L2}{L2} + \frac{\Delta L1\Delta L2}{L1L2} = \varepsilon_{L1} + \varepsilon_{L2} + \varepsilon_{L1}\varepsilon_{L2} \tag{4-9}$$

The linear strain in coal or shale is typically less than 3% at 750 psi in CO_2 and 1% at 1000 psi at helium. Therefore, the high order items, such as$\varepsilon_{L1}\varepsilon_{L2}$, $\varepsilon_{L1}\varepsilon_{L3}$, $\varepsilon_{L2}\varepsilon_{L3}$, $\varepsilon_{L1}\varepsilon_{L2}\varepsilon_{L3}$ could be neglected. After simplification, the volumetric strain and areal strain are reduced to the following form:

$$\varepsilon_V = \varepsilon_{L1} + \varepsilon_{L2} + \varepsilon_{L3} \tag{4-10}$$

$$\varepsilon_A = \varepsilon_{L1} + \varepsilon_{L2} \tag{4-11}$$

Assumption for coal

Coal is typically seen as anisotropic because of the layered characteristic on a large scale. However, as the size comes down to millimeter level, an isotropic condition is assumed based on the description from levine (1996) and Liu and Harpalani (2013). In the literature, linear strains for three dimensions were measured. The calculated volumetric strain was about 3 times the linear strain, which supports that fact that the coal sample could be treated as isotropic in small size. The linear strain is same in both direction:

$$\varepsilon_L = \varepsilon_{L1} = \varepsilon_{L2} = \varepsilon_{L3} \tag{4-12}$$

Therefore, the volumetric strain:

$$\varepsilon_V = 3\varepsilon_L = 1.5\varepsilon_A \tag{4-13}$$

Assumption for shale

No sorption induced strain data of shale were reported. In the experiment, the specimens parallel to bedding (a) and perpendicular to bedding (b) are prepared. Assuming strain within the surface is the same:

$$\varepsilon_{Aa} = \varepsilon_{L1} + \varepsilon_{L2} = 2\varepsilon_{L1} \tag{4-14}$$

$$\varepsilon_{Ab} = \varepsilon_{L2} + \varepsilon_{L3} \tag{4-15}$$

where, ε_{Aa} is the areal strain of sample a, ε_{Ab} is the areal strain of sample b. Therefore, the volumetric strain becomes:

$$\varepsilon_V = \varepsilon_{L1} + \varepsilon_{L2} + \varepsilon_{L3} = 0.5\varepsilon_{Aa} + \varepsilon_{Ab} \tag{4-16}$$

CHAPTER 5

EXPERIMENTAL RESULTS AND DISCUSSIONS

A series of experiments were conducted to measure the areal strain of Hazelton coal, San Juan coal and Marcellus shale with carbon dioxide and helium injections using optical-based method. The results of the induced strain versus injecting gas pressures were presented and reported in this chapter. Some unique features of strain data of shale were observed in the experiment.

5.1 Experimental and Modeled Results

In this section, the sorption-induced strain data versus pressure is presented for two types of coal and Marcellus shale with helium and carbon dioxide separately.

5.1.1 Results of San Juan Coal

Helium Injection Results

Figure 5-1 shows the areal strain for the sample tested for increasing helium pressure. As expected, the area of surface was decreasing with increasing helium pressure due to the mechanical compression. A linear relationship was able to describe the areal strain as a function of pressure perfectly:

$$\varepsilon_A = -0.000137P \tag{5-1}$$

Since the size of sample and strain are both very small, based on equation 4-13:

$$\varepsilon_V = 1.5\varepsilon_A = -0.000206P \tag{5-2}$$

Therefore, based on the definition of C_S (Liu and Harpalani, 2014), the solid matrix compressibility (C_S) was calculated to be -2.06×10^{-4} MPa^{-1} for San Juan coal. This solid matrix compressibility is large which means the specimen was easy to be compressed and softened. This finding consists with the previous results given by different researchers which indicates this optical method is valid for the strain mapping.

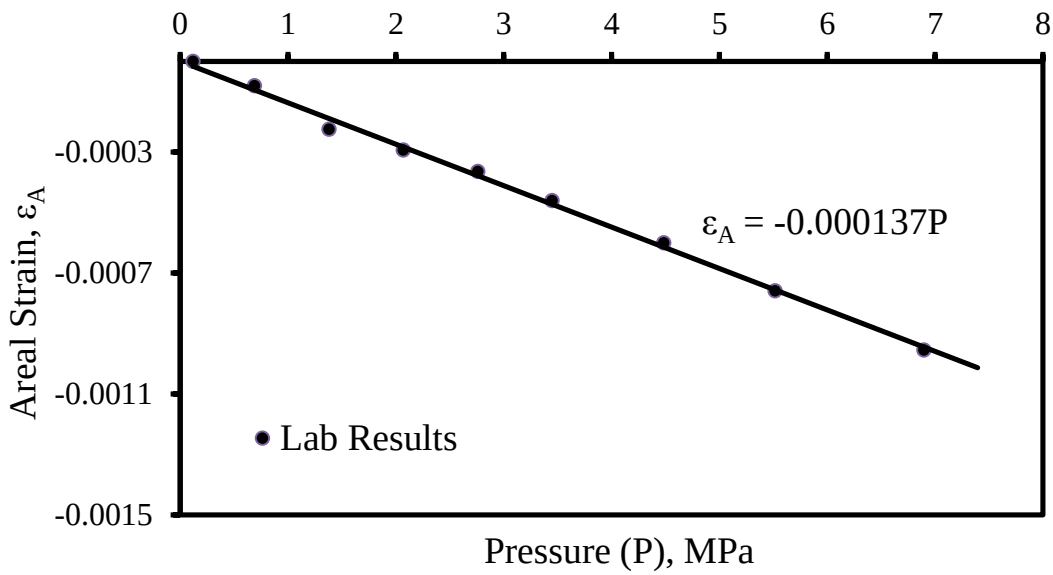

Figure 5.1: Areal strain for San Juan coal with increasing helium pressure

Carbon Dioxide Injection Results and Langmuir Fitting

Figure 5.2 shows the areal strain for increasing carbon dioxide pressure. As expected, the strain data have a strong similarity to typical sorption isotherm. Therefore, the strain was fitted by Langmuir-type strain model (Levine, 1996), given as

$$\varepsilon_L=\varepsilon_M\times P/(P+P_\varepsilon) \tag{5-3}$$

In which ε_L is linear sorption strain at pressure P. ε_M is the theoretically maximum linear strain in infinite pressure. P_ε represents the pressure at which the object has reached 50% of its

maximum strain. In the experiment, areal strain was measured instead of linear strain. Due to the additive property, the Langmuir-type strain model is able to apply to areal strain as well, given as:

$$\varepsilon_A = \varepsilon_{MA} \times P/(P + P_\varepsilon) \quad (5\text{-}4)$$

In which ε_A is areal sorption strain at pressure P. ε_{MA} is the theoretical maximum areal strain in infinite pressure. The value of P_ε and ε_{MA} were 5.24 and 0.0299 respectively.

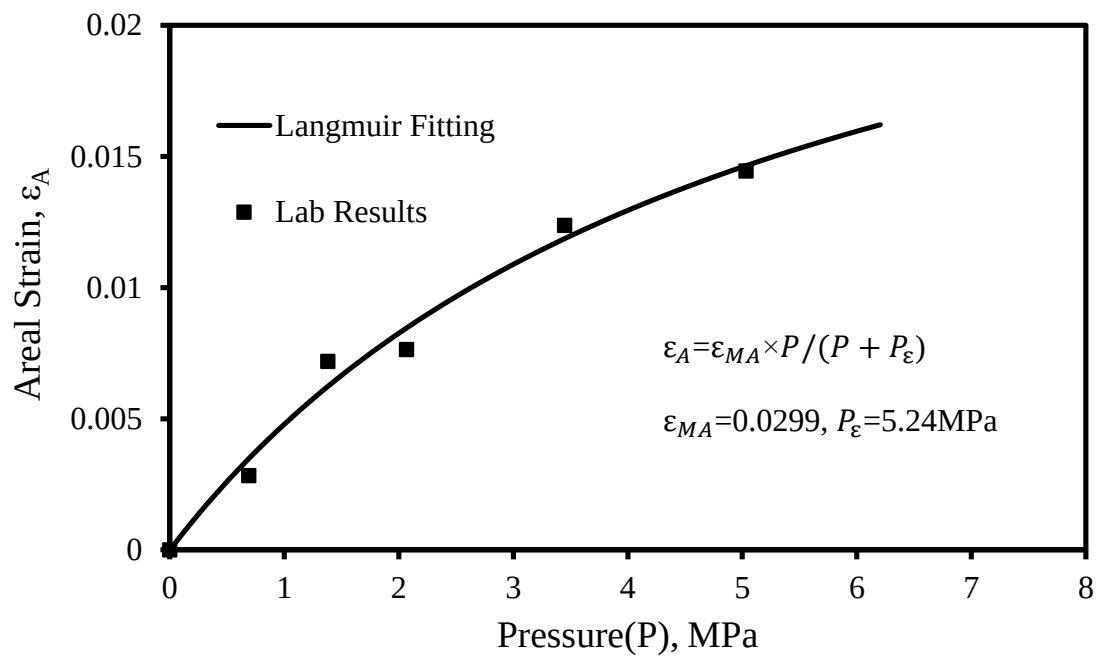

Figure 5.2: Areal strain for San Juan coal with increasing CO_2 pressure

Absolute Sorption-induced Strain

For coal, the areal strain was governed by both mechanical compression and sorption-induced swelling. The helium-induced strain was purely due to mechanical compression. The CO_2-induced strain is considered to be overall strain including both compression-induced strain and sorption-induced strain. Therefore, strain purely caused by sorption could be calculated by

subtracting the compression-induced strain from the overall strain fitted by Langmuir-type equation. Figure 5-3 shows the calculated absolute sorption-induced swelling which can be expressed mathematically as

$$\varepsilon_A = 0.0299 \times \mathrm{P}/(\mathrm{P} + 5.24) + 0.000137\mathrm{P} \quad (5\text{-}5)$$

Based on the assumption made by Levine (1996), absolute sorption-induced volumetric strain was given as

$$\varepsilon_V = 1.5 \times \varepsilon_A = 0.04485 \times \mathrm{P}/(\mathrm{P} + 5.24) + 0.0002055\mathrm{P} \quad (5\text{-}6)$$

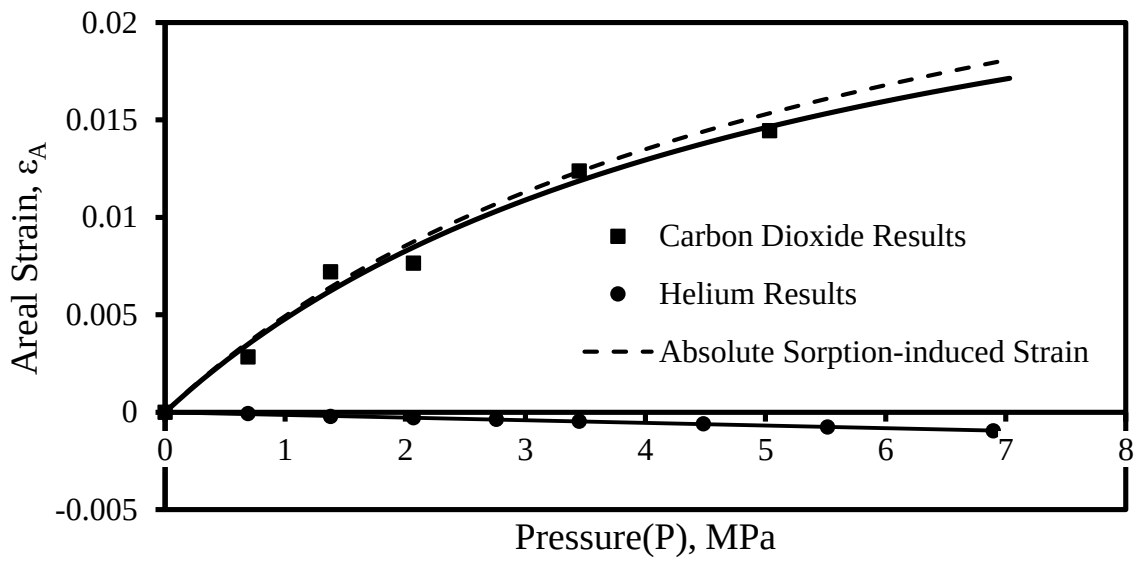

Figure 5.3: Calculated absolute sorption-induced strain for San Juan coal

5.1.2 Results of Hazelton Coal

Helium Injection Results

The experimental procedure was identical as that of San Juan coal. As expected, with increasing helium pressure, the strain was decreasing. Figure 5.4 shows the relationship between pressure and strain. Although some deviation exists, a linear relationship between the strain and

pressure was obvious. Therefore, the soild matrix compressibility of Hazelton coal is calculated to be -1.38×10^{-4} MPa^{-1}. This solid compressibility indicates the coal is hard to compress which is as expected.

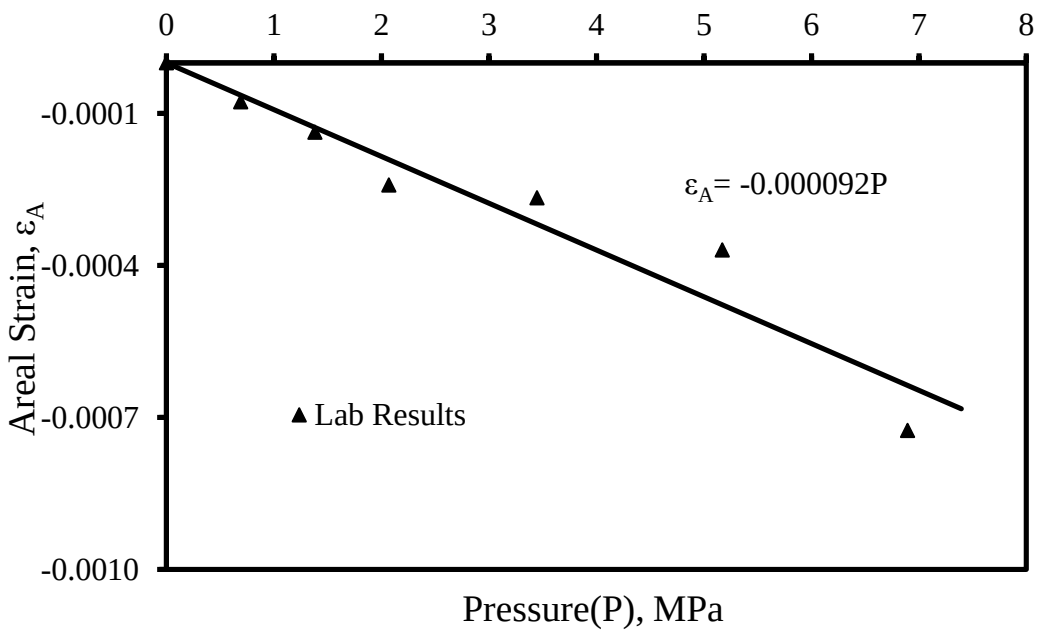

Figure 5.4: Areal strain for Hazlton coal with increasing helium pressure

Carbon Dioxide Injection Results

Similar to results of San Juan coal, the results of Hazlton coal were fitted using Langmuir Fitting perfectly. The value of P_ε and ε_{MA} were 1.704 MPa and 0.01635 respectively.

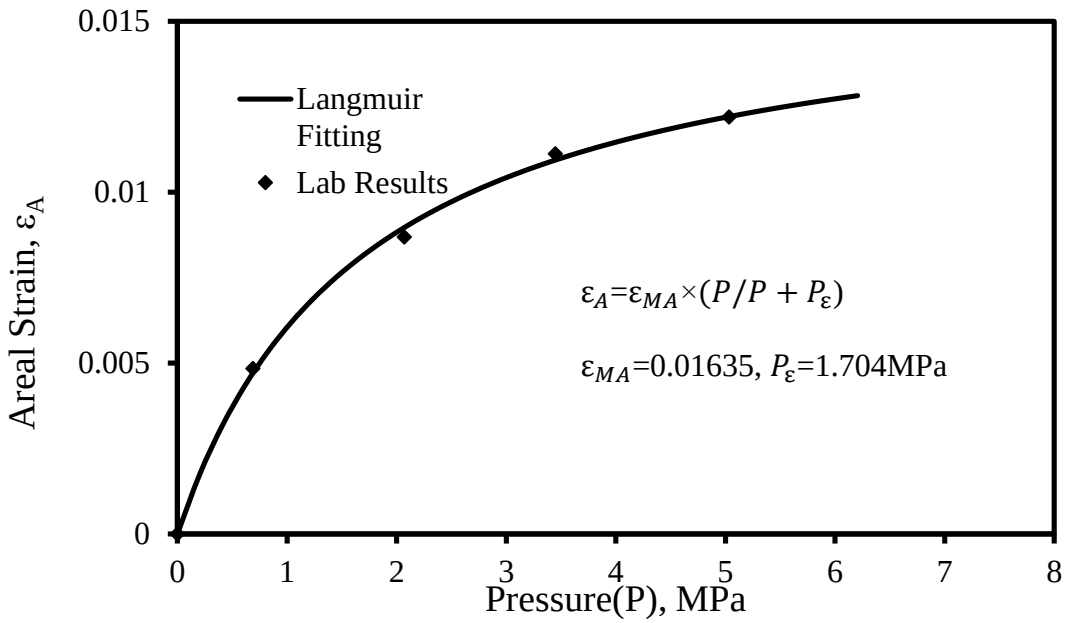

Figure 5.5: Areal strain for Hazlton coal with increasing CO_2 pressure

Absolute Sorption-induced Strain

Based on the same principles and assumptions used in San Juan Coal, absolute sorption-induced strain for Hazelton coal could be calculated. Figure 5.6 shows the calculated absolute sorption-induced areal strain which can be expressed mathematically as

$$\varepsilon_A = 0.01635 \times \mathrm{P}/(\mathrm{P} + 1.704) + 0.000092\mathrm{P} \quad (5\text{-}7)$$

Based on equation 4-13, absolute sorption-induced volumetric strain was given as

$$\varepsilon_V = 1.5 \times \varepsilon_A = 0.02453 \times \mathrm{P}/(\mathrm{P} + 5.24) + 0.000138\mathrm{P} \quad (5\text{-}8)$$

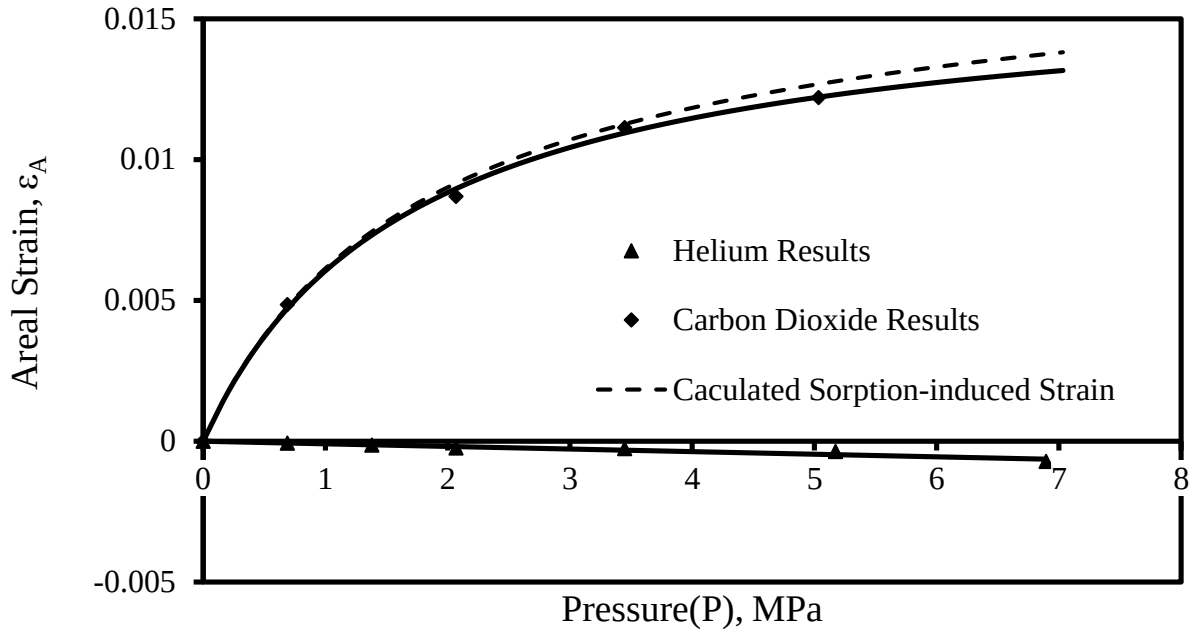

Figure 5.6: Calculated absolute sorption-induced strain for Hazelton coal

5.2 Relationship between Strain and Coal Rank

Sorption capacity of coal is generally thought to increase with rank. The pore size distribution and pore structure are different in coal of different rank. Typically, high-rank coals have larger surface area than low-rank coals, resulting in high sorption capacity in high-rank coal (Seidle, 2011). Sorption-induced swelling/shrinkage is positively proportional to sorption capacity. Therefore, sorption-induced strain is expected to increase with increase of coal rank.

In this study, when the injection pressure is below 2.48 MPa, the amount of adsorption-induced strain for anthracite is higher than the San Juan bituminous coal. However, then the pressure goes above 2.48 MPa, the San Juan coal swells more than anthracite does. The comparison of the absolute sorption-induced strains for San Juan coal and Hazelton coal are showed in figure 5.7. Since the San Juan coal is softer than Hazelton coal, solid matrix

compressibility of San Juan coal is $-2.06\times10^{-4}MPa^{-1}$ which is 1.5 times larger than that of Hazelton Coal, measuring as 1.38×10^{-4} MPa^{-1}. This comparison suggests the coal swelling does not only depend on the coal rank and the other petrophysical properties, such as micro-structure, pore size distribution, fixed carbon content, should also be considered for the shrinkage/swelling analysis.

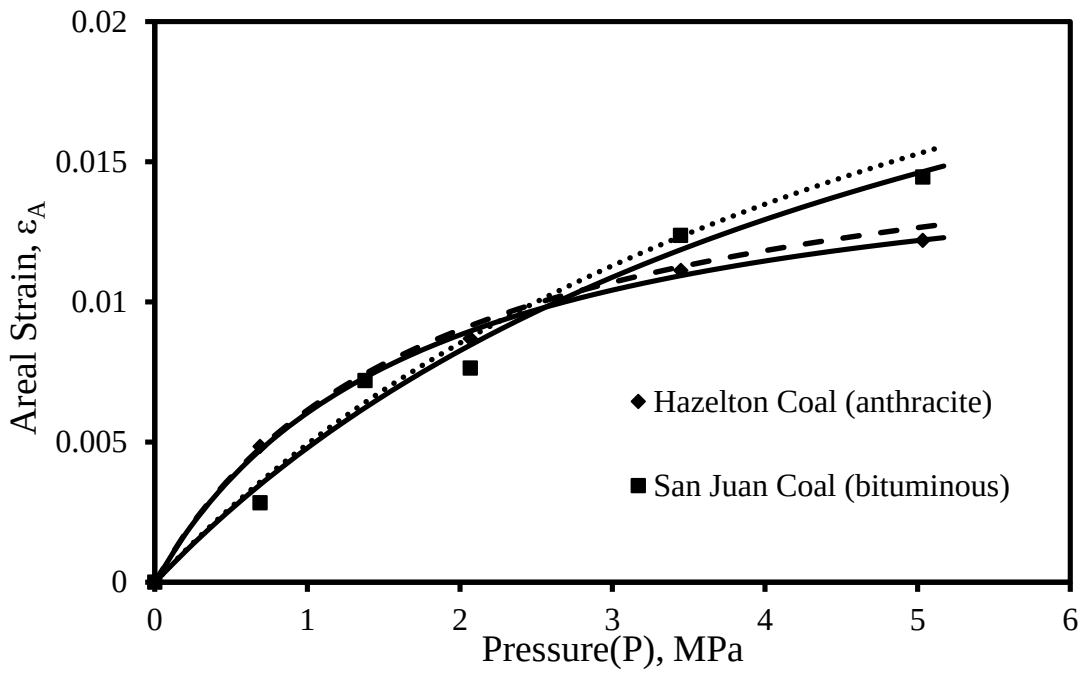

Figure 5.7: Strain variation for two different coal specimens

5.3 Model Application and Validation

In this section, the theoretical model developed by Liu and Harpalani (2013) was used to fit the experimental data. The theoretical model was reviewed in Chapter 3. Table 5-1 shows the parameters required for modeling. The temperature (T) was maintained during the experiment at 298.15 K. The adsorption capacities of Same San Juan coal and Hazelton coal were measured. The Langmuir constants (a and b) were calculated from those data. The solid phase density is

chosen as 1.5 t/m^3 for coal. The Poisson's ratio was chosen to be 0.4 and 0.29 respectively, which were thought to be reasonable for coal. The young's modulus (E) was set to 2267 MPa for San Juan coal and 3600 MPa for Hazelton coal. The modulus of solid expansion (E_A) was regressed from the experimental data to be 839 MPa for San Juan coal and 793 MPa for Hazelton coal. Gas molar volume (V_0) and gas constant (R) are needed in the calculation. Because the theoretical model was only applied to linear strain and volumetric strain, the areal strain was converted to linear strain in the model.

Coal Type	T(K)	a(m3/t)	b(MPa-1)	ρ(t/m3)	v
San Juan	298.15	24.35	0.7584	1.5	0.4
	EA(MPa)	E(MPa)	Ratio(E/EA)	V0(L/mol)	R(J*mol-1*K-1)
	839	2267	2.7	22.4	8.314
Coal Type	T(K)	a(m3/t)	b(MPa-1)	ρ(t/m3)	v
Hazelton	298.15	29.77	0.4657	1.5	0.2
	EA(MPa)	E(MPa)	Ratio(E/EA)	V0(L/mol)	R(J*mol-1*K-1)
	793	3600	4.5	22.4	8.314

Table 5.1: Input parameters required for modeling of different coal types

Figure 5.8 shows the modeled results along with the experimental data for the linear strain of San Juan coal as a function of pressure.

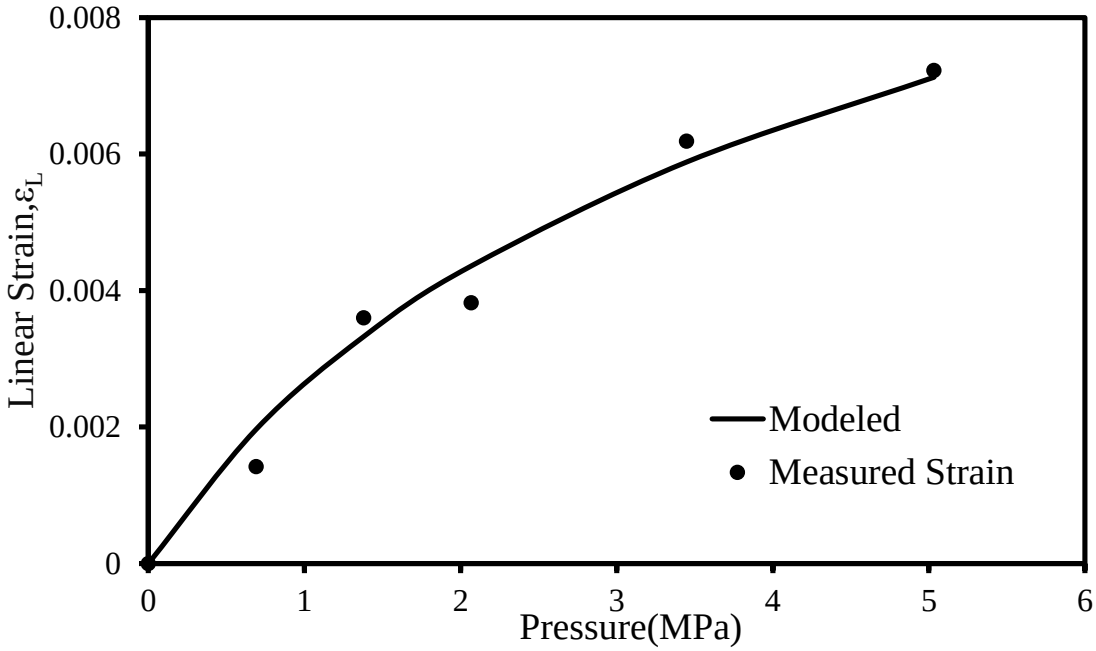

Figure 5.8: Modeled adsorption-induced strain for San Juan coal

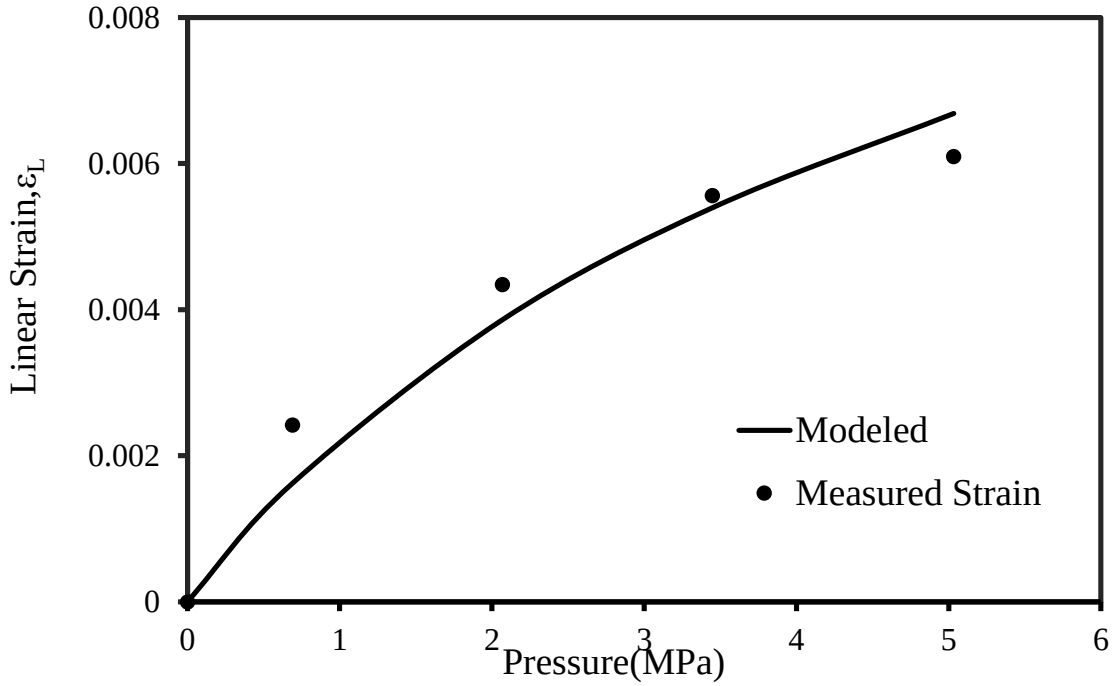

Figure 5.9: Modeled adsorption-induced strain for Hazelton coal

Figure 5.9 shows the modeled results of Hazelton coal. The measured linear strain is fitted well with the modeled strain by choosing the reasonable rock properties.

Based on the modeled results, Liu and Harpalani model (2013) works well with reasonable input parameters for carbon dioxide sorption. This finding confirms that energy balance method is valid for both methane and CO_2 injections. This allows Liu and Harpalani model to be applied for multi-component gases which will be shred the light on the carbon sequestration in depleted CBM reservoir fields. Additionally, this model also can be applied on higher rank coals such as anthracite. This finding is critical for the carbon sequestration in higher rank coals such as abandon anthracite coal seams in Pennsylvania and unmineable anthracite coal seams.

5.4 Experimental Results of Marcellus Shale

Figure 5.10 shows the helium injection results, two samples with different direction were used and the linear relationship could describe the strain as a function of pressure.

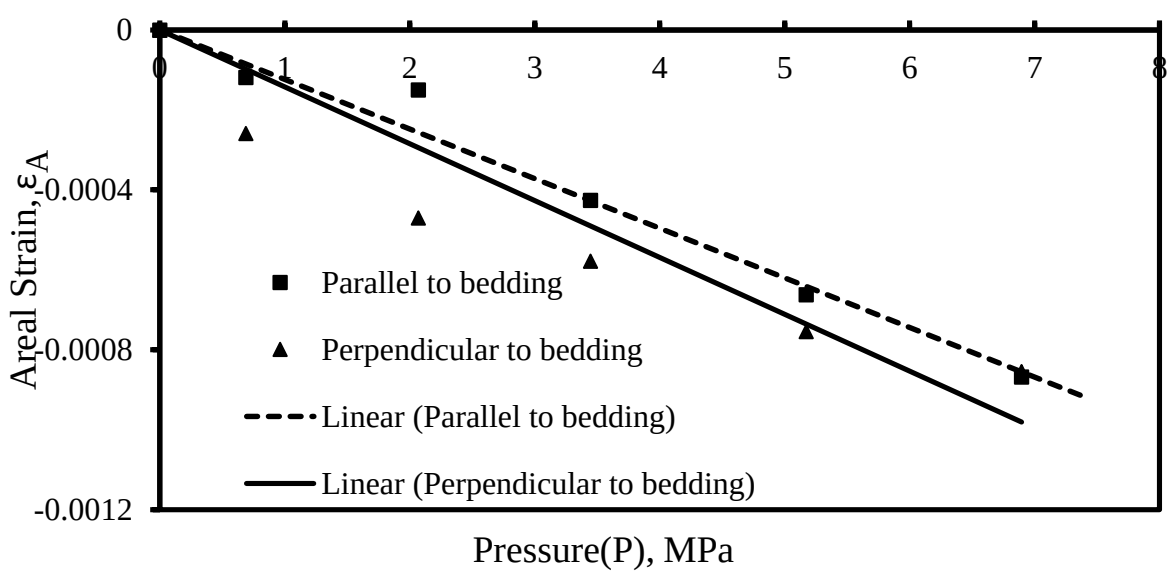

Figure 5.10: Areal strain for Marcellus shale with increasing helium pressure

After completing the helium cycle, CO_2 was injected to see the swelling effect of shale sample. Each test was repeated and average value were used. Figure 5.11 shows the results. Unlike the strain data with CO_2 –coal injection, strain data with increasing CO_2 for shale is not typically Langmuir-type trend. Surprisingly, at low pressure (0.69MPa), the negative strains were observed for both specimens. It indicates the specimens shrink when the gas pressure is low, which might imply that the overall deformation is dominated by mechanical compression. If the gas injection pressure kept increasing, the positive strains were measured for both specimens. This might be due to the sorption-induced strain exceeds the mechanical induced strain. This finding is unexpected. It might be attributed to the complex micro-structure of shale and/or the complex mineral composition which includes a significant amount of clay minerals. Future research will be required to explain this phenomenon.

In terms of the strain modeling for shale, it is quite challenging to extend Liu and Harpalani model for shale shrinkage and swelling since the model cannot address the negative strain behavior. If the model can take the dynamic moduli into account, it might be applicable for shale strain prediction. Future research will be needed to model the sorption-induced shale strains profiles.

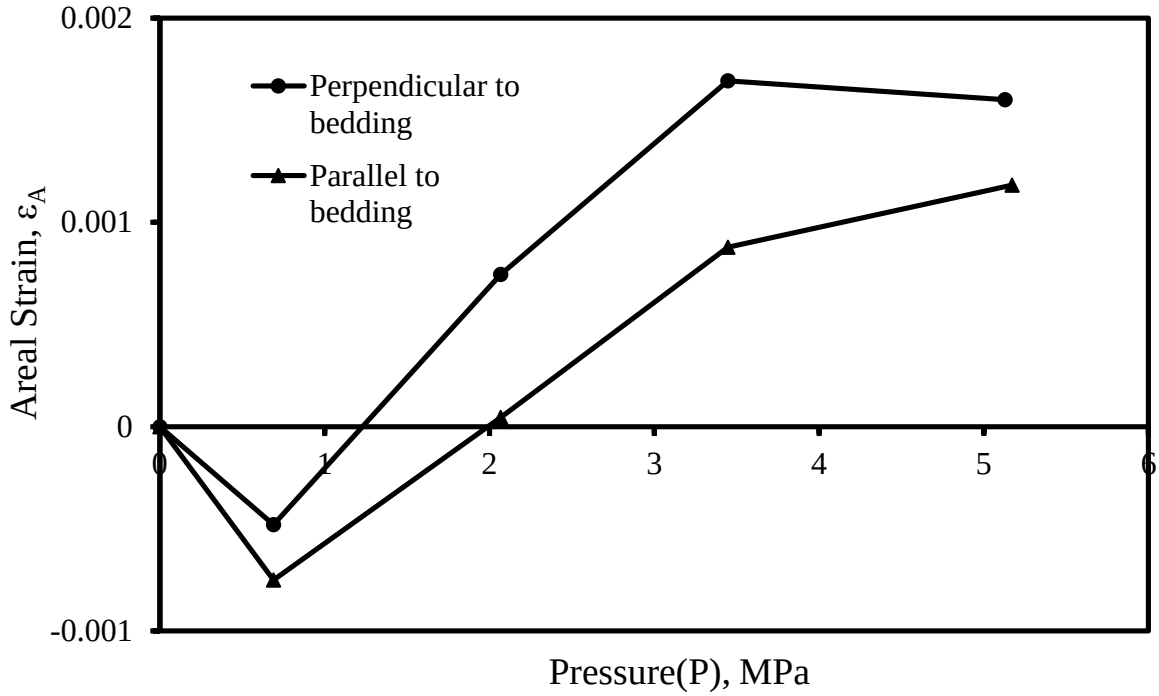

Figure 5.11: Areal strain for Marcellus shale with increasing CO_2 pressure

5.5 SEM Results of Marcellus Shale

The sample is the core from the deep Marcellus formation. The matrix in Marcellus shale consists of organic matter and inorganic matters such as carbonate grains, quartz grains and clay minerals. Figure 5.12 shows the minerals in Marcellus shale, in which the light-gray regions represent inorganic minerals and dark-grey regions represent organic matter. Framework pores, or inorganic pores, are unique in shale. Those pores are made of triangular pores range from 10nm to more than a micrometer and tend to be best developed in areas that were protected from the force of compaction pressure. Protected areas occur in pressure shadows adjacent to large compaction-resistant, rigid grains.

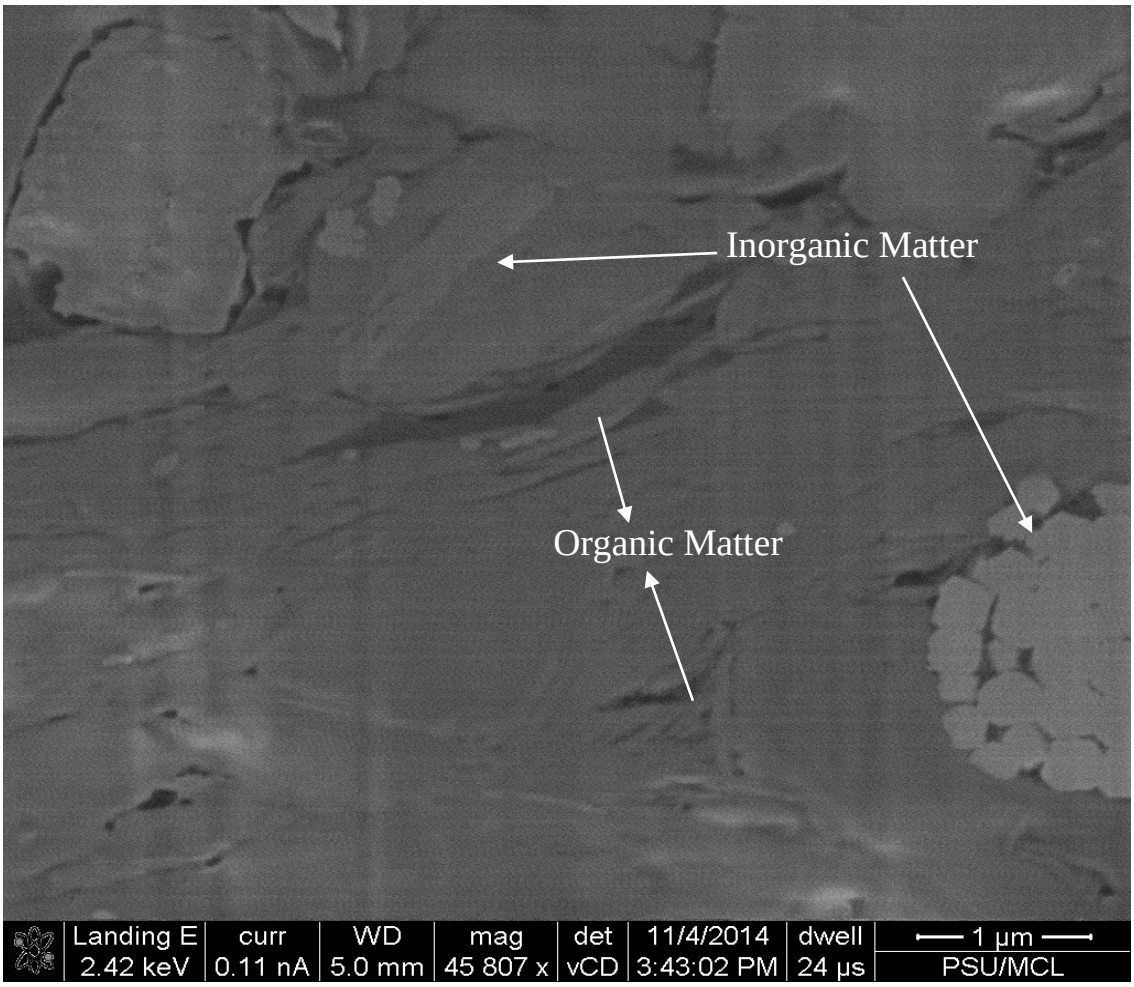

Figure 5.12: Organic matter and inorganic matter in Marcellus shale

Pores in organic matter occur in all samples and are restricted to the unstructured, amorphous organic matter. Amorphous organic matter may include material that was partially degraded by microbes, is disseminated throughout the rock matrix, and also fills open spaces in fossil cavites. Structure kerogen is devoid of organic matter pores. Amorphous kerogen contains abundant pores in the thermally mature Marcellus shale samples. Figure 5.13 shows the inorganic pores and organic pores in Marcellus shale sample. As we can see in Figure 5.13, the organic pores are typically within 50 nm and the inorganic pores are much larger.

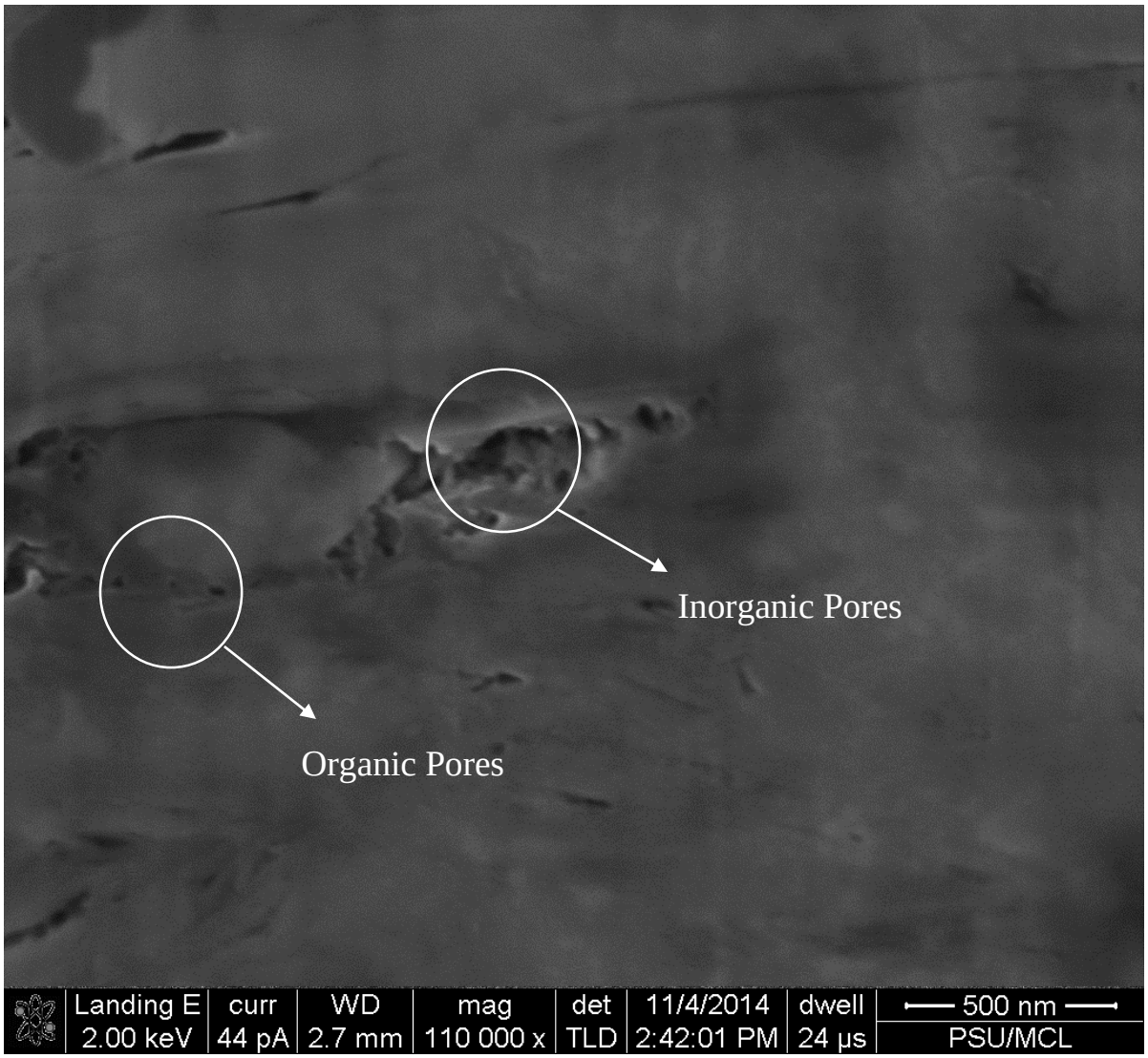

Figure 5.13: Pores in organic matter and inorganic matter in Marcellus shale

5.6 Discussions

By using the new developed optical apparatus, the areal strain of two coal specimens was measured. For carbon dioxide at 5.03 MPa, the areal strain was about 1.4% and 1.2% of San Juan coal and Hazelton coal respectively. Harpalani and Mitra (2009) measured the volumetric strain of San Juan coal was about 1.1% for CO_2 at 5MPa. Robertson and Eric (2005) showed that the longitude strain of a bituminous coal is around 0.8% at 5MPa. The difference in the experiment is that Harpalani and Mitra used strain gauge in the measurement; Robertson and Eric, however,

recorded the deformation using optical method, which is different from current plan. Assume homogeneous in small coal sample, linear strain of current work is 0.7% and that of Harpalani and Mitra's data is about 0.37%. The results showed that strain measured by optical method is obviously larger than that measured by strain gauge for same rank of coal. This could be explain qualitatively that the cleats swell less than the matrix, which has been reported in Zeng et al (2015). In their work, the internal swelling ratio is always less than 1; therefore, the big block with a lot of cleats could have smaller swelling strain than small sample without cleats or with just a few cleats. The other thing is that glue may resist the deformation of matrix or cleats. Robertson and Eric (2005) have developed an optical measurement apparatus to measure the strain, but they measured the strain by calculating the change of pixels when the end of sample moved; however, gas flow itself might move the sample. Although the possibility is small, it might affect the accuracy of measurement. In current work, with the use of telecentric lens, the error caused by gas flow could be avoided.

By reducing the shale sample size to about 3mm*3mm*1mm cubic, the equilibrium time could be reduced significantly; by using the optical strain measurement apparatus, the challenge related to small strain is overcome.

The negative strains were observed at low pressure gas injection for Marcellus shale. A hypothesis was proposed to explain the phenomenon. The volumetric swelling strains of clays were not linear to the adsorption capacity of CO_2. Instead, with the increasing adsorption capacity, the rate of deformation is speeded up. That fact might imply that in low pressure, the absolute sorption-induced strain is very low so the compression dominates, and with pressure increase, absolute sorption-induced strain is increasing rapidly, then dominating the strain finally. This hypothesis is confirmed by the data from Heller and Zoback (2014), where the

swelling rate of clay is increasing with pressure. The shale consists of both clays and organic matter which also swells. Compared to organic matter, the clay minerals are relatively hard. It is easy to believe that the strain is dominated by the clay swelling instead of organic matter. Therefore, the relationship between clay swelling and overall swelling should be realized by measuring the strain of each component separately. Although not thoroughly understood, the results show the swelling phenomenon of real shale and the magnitude of it, which may play an important role in gas transport properties during shale gas production.

CHAPTER 6

CONCLUSIONS AND FUTURE WORK

6.1 Conclusions and Summary

The following conclusions have been drawn from this study:

1. The new designed optical apparatus works well for the measurement of areal strain of millimeter-sized coal and shale specimens. The precision is about 10^{-5} which is enough for detecting the small deformation in coal and shale.
2. Using this optical-based strain measurement apparatus, two shortcomings by using strain gauges are overcome. Firstly, without chemical glue, the strain could be measured directly, which largely improves the accuracy of measurement. Secondly, the specimens are deliberately made in small size in order to reduce the influence of built-in cleats.
3. The results of coal show that adsorption-induced strain isotherms are fitted perfectly with Langmuir-type equation. Liu and Harpalani model was also used to match the data and the modeled results well match the strain data with reasonable rock properties. For CO_2 at 5MPa, the areal strain is about 1.4% and 1.2% of San Juan coal and Hazelton coal respectively. At 5MPa CO_2, therefore, the linear strain of San Juan coal is 0.7% in current work but the value measured by strain gauges in open literature is 0.37% for the sample in same basin, which is expected.
4. With injection of CO_2, Hazelton coal, an anthracite coal, swelled more in relatively low pressure (<2.48MPa) than San Juan coal, a bituminous coal. In relatively high pressure (>2.48MPa), San Juan coal, however, swelled more than Hazelton coal. The comparison

suggests that coal swelling depends not only on rank but also other petrophysical properties, such as micro-structure, pore size distribution and fixed carbon content.

5. The results of shale shows that the adsorption-induced strain isotherms are not typical Langmuir-type isotherms. At 0.69MPa CO_2, the negative strain was observed. This might imply that in low pressure, the adsorption-induced swelling was very low and fully offset by the mechanical compression. With injection pressure increase, the adsorption-induced swelling began to dominate the overall strain and the maximum strain of 0.18% was observed for the tested shale specimens.

6.2 Future Work

In future work, the more detailed sorption-induced strain of shale need to be measured. Unlike coal, which is relatively simple in composition, shale typically consists of organic matter, clays, and other minerals. Both organic matter and clays have adsorption effect. Therefore, the sorption-induced strains in organic matter and clays need to be measured respectively by special method, such as neutron diffraction, in order to thoroughly understand the overall swelling behavior.

REFERENCES

Akkutlu, I. Y., & Fathi, E. (2012). Multiscale Gas Transport in Shales with Local Kerogen Heterogeneities. *SPE Journal*, *17*(4), 1002–1011.

Aljamaan, H., Alnoaimi, K., & Kovscek, a. R. (2013). In-Depth Experimental Investigation of Shale Physical and Transport Properties. *Unconventional Resources Technology Conference, Denver, Colorado, 12-14 August 2013*, 1120–1129

Anggara, F., Sasaki, K., Rodrigues, S., & Sugai, Y. (2014). The effect of megascopic texture on swelling of a low rank coal in supercritical carbon dioxide. *International Journal of Coal Geology*, *125*, 45–56.

Brunauer, S., Emmett, P. H., & Teller, E. (1938). Adsorption of Gases in Multimolecular Layers. *Journal of the American Chemical Society*, *60*(2), 309–319.

Chalmers, G. R., Bustin, R. M., & Power, I. M. (2012). Characterization of gas shale pore systems by porosimetry, pycnometry, surface area, and field emission scanning electron microscopy/transmission electron microscopy image analyses: Examples from the Barnett, Woodford, Haynesville, Marcellus, and Doig units. *AAPG Bulletin*, *96*(6), 1099–1119.

Cui, X., Bustin, a. M. M., & Bustin, R. M. (2009). Measurements of gas permeability and diffusivity of tight reservoir rocks: Different approaches and their applications. *Geofluids*, *9*(3), 208–223

Civan, F., Rai, C. S., & Sondergeld, C. H. (2011). Shale-Gas Permeability and Diffusivity Inferred by Improved Formulation of Relevant Retention and Transport Mechanisms. *Transport in Porous Media*, *86*(3), 925–944.

Curtis, J. B., & Curtis, J. B. (2002). Fractured shale-gas systems, *11*(11), 1921–1938.

Curtis, M. E., Ambrose, R. J., Sondergeld, C. H., & Rai, C. S. (2010). Structural Characterization of Gas Shales on the Micro- and Nano-Scales. *Canadian Unconventional Resources & International Petroleum Conference*, (October), 1–15.

Gray, I. (1987). Reservoir engineering in coal seams: part 1 - The physical process of gas storage and movement in coal seams. *SPE Reservoir Evaluation & Engineering*, *2*(1), 28–34.

Haenel, M. W. (1992). Recent progress in coal structure research. *Fuel*, *71*(11), 1211–1223.

Hao, F., Zou, H., & Lu, Y. (2013). Mechanisms of shale gas storage: Implications for shale gas exploration in China. *AAPG Bulletin*, *97*(8), 1325–1346.

Harpalani, S., & Chen, G. (1997). Influence of gas production induced volumetric strain on permeability of coal.pdf, 303–325.

Harpalani, S., & Mitra, A. (2010). Impact of CO2 injection on flow behavior of coalbed methane reservoirs. *Transport in Porous Media*, *82*(1), 141–156.

Harpalani, S., Prusty, B. K., & Dutta, P. (2006). Methane/CO2 sorption modeling for coalbed methane production and CO2 sequestration. *Energy and Fuels*, *20*(4), 1591–1599.

Harpalani, S., & Schraufnagel, R. (1990). Shrinkage of coal matrix with release of gas and its impact on permeability of coal. *Fuel*, *69*(5), 551–556.

Heller, R., & Zoback, M. (2014). Adsorption of methane and carbon dioxide on gas shale and pure mineral samples. *Journal of Unconventional Oil and Gas Resources*, *8*(0), 14–24.

Kulander, B. R., & Dean, S. L. (1993). Coal-cleat domains and domain boundaries in the Allegheny Plateau of West Virginia. *AAPG Bulletin*, *77*(8), 1374–1388. Retrieved from http://aapgbull.geoscienceworld.org/cgi/content/long/77/8/1374

Langmuir, I. (1916). the Constitution and Fundamental Properties of Solids and Liquids. Part I. Solids. *Journal of the American Chemical Society*, *252*.

Langmuir, I. (1918). The Adsorption of Gases on Plane Surfaces of Glass, Mica and Platinum. *Journal of the American Chemical Society*, *40*(9), 1361–1403. http://doi.org/doi: 10.1021/ja02242a004

Laubach, S. E., Marrett, R. a., Olson, I. E., & Scott, a. R. (1998). Characteristics and origins of coal cleat: a review. *International Journal of Coal Geology*, *35*(1-4), 175–207.

Levine, J. R. (1996). Model study of the influence of matrix shrinkage on absolute permeability of coal bed reservoirs. *Geological Society, London, Special Publications*

Lin, W. (2010). Gas Sorption and the Consequent Volumetric and Permeability Change of Coal, (March).

Liu, S. (2012). Estimation of Different Coal Compressibilities of Coalbed Methane Reservoirs Under Replicated in Situ Condition, (May), 141.

Liu, S., & Harpalani, S. (2013). A new theoretical approach to model sorption induced coal shrinkage or swelling. *AAPG Bulletin*, *7*(7), 1033–1049.

Liu, S., & Harpalani, S. (2014). Compressibility of Sorptive Porous Media: Part II – Experimental Study on Coal. *AAPG Bulletin*, *9*(9), accepted.

Navitar. (2013). 12X Zoom High Mag Zoom Lenses. Navitar. Rochester, NY.

Nyahay, R., Leone, J., Smith, L., Martin, J., & Jarvie, D. (2007). Update on Regional Assessment of Gas Potential in the Devonian Marcellus and Ordovician Utica Shales of New York.

Pan, Z., & Connell, L. D. (2007). A theoretical model for gas adsorption-induced coal swelling. *International Journal of Coal Geology*, *69*(4), 243–252.

Pashin, J. C. (2008). Coal as a petroleum source rock and reservoir rock.*Applied coal petrology: The role of petrology in coal utilization (eds I. Suárez-Ruiz and JC Crelling)*, 227-262.

Polanyi, M. (1963). The Potential Theory of Adsorption. *Science (New York, N.Y.)*, *141*(3585), 1010–1013

Rightmire, C. T. (1984). Coalbed methane resource.

Robertson, E. P. (2005). Measurement and Modeling of Sorption- Induced Strain and Permeability Changes in Coal. *Contract*, (October).

Ross, D. J. K., & Marc Bustin, R. (2007). Impact of mass balance calculations on adsorption capacities in microporous shale gas reservoirs. *Fuel*, *86*(17-18), 2696–2706.

Schettler, P., Parmely, C. R., & Lee, W. J. (1989). Gas Storage and Transport in Devonian Shales. *SPE Formation Evaluation*, *4*(3), 371–376.

Seidle, J., & Huitt, L. (1995). Experimental measurement of coal matrix shrinkage due to gas desorption and implications for cleat permeability increases. *International Meeting on Petroleum Engineering*.

Seidle, J. (2011). *Fundamentals of coalbed methane reservoir engineering*. PennWell Books.

Smith, D.M.& Williams, F.L.(1984). Diffusion effects in the recovery of methane from coalbeds. *SPE Journal*, *24*, 529-535.

St. George, J. ., & Barakat, M. . (2001). The change in effective stress associated with shrinkage from gas desorption in coal. *International Journal of Coal Geology*, *45*(2-3), 105–113.

Staib, G., Sakurovs, R., & MacA Gray, E. (2014). Kinetics of coal swelling in gases: Influence of gas pressure, gas type and coal type. *International Journal of Coal Geology*, *132*, 117–122.

U.S.EIA (Energy Information Administration). (2014). Coalbed Methane Production. Accessed June 6, 2015, http://www.eia.gov/dnav/ng/ng_prod_coalbed_s1_a.htm.

U.S.EIA (Energy Information Administration). (2014). Dry Natural Gas Production. Accessed June 6, 2015, http://www.eia.gov/dnav/ng/hist/n9070us2m.htm.

U.S.EIA (Energy Information Administration). (2014). Shale Gas Production. Accessed June 6, 2015, http://www.eia.gov/dnav/ng/ng_prod_coalbed_s1_a.htm.

Yang, R. T. (2013). *Gas separation by adsorption processes*. Butterworth-Heinemann.

Zang, J., Wang, K., & Zhao, Y. (2015). Evaluation of gas sorption-induced internal swelling in coal. *Fuel*, *143*, 165–172.